Natural Modes of Liquid Sloshing in a Cylindrical Container with an Elastic Cover

K. Ren [a], G.X. Wu [a, †], Z.F. Li [b]

[a] *Department of Mechanical Engineering, University College London, Torrington Place, London WC1E 7JE, United Kingdom*

[b] *School of Naval Architecture and Ocean Engineering, Jiangsu University of Science and Technology, Zhenjiang 212003, China*

† Corresponding author: G.X. Wu (g.wu@ucl.ac.uk)

Abstract

Liquid sloshing and its interaction with an elastic cover in a cylindrical tank is considered. The velocity potential for the fluid flow is expanded into the Bessel-Fourier series as commonly used. An efficient scheme is then developed, which allows the plate deflection to use the same type of expansion as the potential. When these two series are matched on the interface of the fluid and the plate, the unknown coefficients in the two expansions can be easily obtained. This is much more convenient than the common procedure where a different expansion is used for the plate and upon matching each term in the series of the plate is further expanded into the series used for the potential. Through the developed method, an explicit equation is derived for the natural frequencies and extensive results are provided. The corresponding natural mode shapes and principal strains distribution of the elastic cover are also investigated. Results are provided and the underlining physics is discussed. To verify the obtained results, the problem is also solved through a different method in which the potential is first expanded into vertical modes. Another explicit equation for the natural frequencies is derived. While the equation may be in a very different form, through the residual theorem, it is found that the second equation is identical to the first one.

Key words: coupled fluid/structure vibration; natural modes; sloshing; elastic cover; eigenfunctions expansion.

1. Introduction

Liquid sloshing commonly exists in nature. It can also often be observed in many engineering applications, such as in marine transportation of crude oil and liquefied natural gas (LNG) (Rognebakke and Faltinsen [1]; Mitra et al. [2]), oil/LNG storage on land undergoing earthquakes (Hatayama [3]), motions of liquid fuel in spacecrafts and aircrafts (Veldman et al. [4]; Farhat et al. [5]), and bulk liquid road transportation (Toumi et al. [6]). Sloshing motions in many cases have adverse effect, which sometimes could have server consequence. This is primarily because the sloshing is usually the liquid motion in a confined container and is caused by the oscillation of the container. When the motions of the container and liquid are synchronized, energy from the container will be continuously transferred to the liquid. The energy of the liquid accumulates, and its motion becomes bigger and bigger, which is commonly known as resonance. In such a case, the large liquid motion may create large loads on the container and it is not uncommon that impact occurs regularly, which generates very high pressure over a short period of time. An example is an LNG carrier navigating on ocean. Violent liquid motion inside the tank may occur especially in the rough seas. When the frequencies of external excitation are close to the natural frequencies of the sloshing containers, the violent fluid motion may not only cause damage to the inner structure of containers, but also affect the motion of ships and pose a threat to their safety. It is therefore important to predict the natural frequencies accurately to help to control resonant motion and to minimize its effect. While the liquid sloshing may have many undesirable effects, it can also be used beneficially. In marine engineering, anti-roll tanks are sometimes installed in ships. The liquid motion can adjust to provide a counter force to improve the seakeeping performance of the ship. Tuned Liquid Damper (TLD) is sometimes installed in high-rise buildings for increasing dampening and decreasing vibration of structures induced by environmental factors such as wind.

Due to its practical importance and relevance, extensive research has been undertaken on liquid sloshing. Based on the velocity potential theory, Faltinsen [7] studied sloshing in a two-dimensional (2D) rectangular tank. For the linear problem [7] derived the

analytical solutions for the natural frequencies and for liquid motion under the forced sway oscillation of the tank, and also solved the corresponding nonlinear problem numerically based on the boundary element method. The same problem was also studied by Nakayama and Washizu [8] and Chen et al. [9] based on boundary element method and finite difference method, respectively. The two-dimensional sloshing problem in a general-shaped tank was considered by Solaas and Faltinsen [10]. The finite element method developed for the 2D nonlinear free surface problem (Wu and Eatock Taylor [11]) was extended to the 3D case and further applied to study the nonlinear sloshing problem in a rectangular tank by Wu et al. [12]. An analytical approach based on a modal theory was adopted by Faltinsen and Timokha [13] to deal with the nonlinear sloshing in a 2D rectangular tank. Based on the perturbation theory, Wu [14] investigated the second-order resonant behaviours of sloshing in a 2D rectangular tank. Wu [14] observed that the second-order resonance would occur when the difference/sum of two excitation frequencies approached to any even mode of natural frequencies. Apart from works mentioned above, there are many others dealing with 2D/3D tanks with different shapes using various solution methods analytically or numerically either based on velocity potential theory or Navier-Stokes equations, which have been summarised in Ibrahim [15] and Faltinsen and Timokha [16].

Apart from sloshing of liquid with a free surface, there are also practical examples where there is an elastic cover on the liquid surface, for example a floating roof over the crude oil storage. Another example is the problem related to “seiche” phenomenon in some ice-covered water areas in cold regions. When the vertical dimension of an elastic cover is much smaller than the horizontal ones, it is common to use elastic plate theory for the cover. The deformation of elastic plate and the motion of liquid are coupled. The natural modes of the coupled system will be very much different from those of system with free surface. For example, Bauer [17] studied the natural frequencies of sloshing liquid in a circular cylindrical container covered by a membrane or plate cover based on the Bessel-Fourier series expansion. In [17], the written deflection of the plate contains two components. One is a special solution of the inhomogeneous equation due to the hydrodynamic pressure, in which the same

orthogonal Bessel-Fourier expansion is used as that for the velocity potential. The other is the general solution of the homogenous equation, in which a different Bessel series is used. This can be clearly seen in the two summations of Eq. (33) of [17]. Amabili [18] considered a circular cylindrical container where the liquid surface is partially covered by an elastic circular plate, with its centre coincident with the centre line of the tank. In [18], the plate deflection and velocity potential are expanded into two different Bessel-Fourier series with unknown coefficients. Different from [17], the expansion for the plate deflection has taken into account the plate edge conditions, and the dynamic condition is imposed based on the Rayleigh-Ritz method. Using the same method, Kim and Lee [19] investigated the case of the liquid surface partially covered by a doughnut-shaped plate with its outer edge clamped to the tank wall. Recently, the problem in [17] was reconsidered by [20] based on the virtually same method, where more mathematical details such as on the coefficient matrix and additional results for simply supported edge cases were provided.

In this paper, we shall consider the natural frequencies and natural modes of liquid in a circular cylindrical tank with an elastic cover on the surface. The edge condition of the cover, or the condition at the intersection of the cover and the tank wall can be arbitrary. Specifically, we shall focus on the clamped, simply supported and free edges, although their combinations can be equally considered. Two efficient methods have been developed, whose procedures can be used more generally for this type of problem.

In the first method, variable separation method is used for the velocity potential which is expanded into a series in the horizontal plane. For a circular cylindrical tank, the expansion is in the form of Bessel-Fourier series which satisfies the tank wall condition. The vertical expansion is then obtained from the solution of the Laplace equation. It satisfies the tank bottom condition but not the conditions on the cover. This part may be similar to that in Bauer [17]. However, a major and significant difference is that Bauer [17] subsequently used two series (one double series plus one single series) for the deflection of the cover, based on respectively the special solution of the inhomogeneous equation and general solution of the homogeneous equation. The latter

differs from that used for the potential. When matching dynamic and kinematic conditions on the interface of the cover and liquid, each term in the series of general solution has to be expanded into the Bessel series of the velocity potential. When the edge conditions are imposed, the unknown coefficients are coupled, and it leads to an infinite set of linear equations. If this is solved directly without further treatment, it has to be truncated at a large finite number and the natural frequencies can be obtained when the determinant of coefficient matrix is zero. A very similar procedure was used in [20].

In the context of the work mentioned above, the novelty of present method can be summarized below. Here we have developed a method through which the deflection w of the plate can be expanded in terms of the same Bessel-Fourier series as that for velocity potential ϕ. This may sound trivial. However, the challenge is that when the expansion is applied to w itself, the operator ∇^4 cannot always be directly applied to the expansion, as the series usually becomes divergent. We have therefore expanded $\nabla^4 w$ instead and developed a procedure to work out the expansion of w based on that of $\nabla^4 w$. This not only avoids the issue of divergence but also provides a means to impose the edge conditions. When w and ϕ are expanded into the same Bessel-Fourier series, their coefficients form a one-to-one relationship because of orthogonality, when matching conditions are imposed. Subsequently, when the edge conditions are enforced, a simple 2-by-2 matrix equations are obtained. The natural frequencies can be obtained when the determinant of this 2-by-2 matrix is zero and this is a very simple operation. In the work of [17] and [20], the infinite matrix $\boldsymbol{A}$ is truncated at a finite value, e.g., M. As M becomes larger, to solve $\det(\boldsymbol{A}) = 0$ directly becomes numerically more difficult. In [20], M is chosen around 10. Here in our work, the matrix is only 2-by-2 and its determinant can be calculated easily. For the results, [17] provided only the clamped case, while [20] further provided simply supported cases. Neither of them provided results for the free edge conditions.

To verify our procedure, a second method is also developed. For the velocity potential, the deflection appears only in its dynamic and kinematic boundary conditions on the cover. Once these two conditions are combined, the deflection can be eliminated and

problem becomes a one for the potential only. The potential is then first expanded in the vertical direction and each term satisfies the tank bottom condition and combined dynamic and kinematic condition on the cover. Through using the inner product and orthogonality, the tank wall and edge conditions are satisfied. As a result, another explicit equation for the natural frequencies is also derived. This equation is in a form very different from that derived from the first method. However, through residual theorem in the complex plane, they are found to be identical.

This paper is organized as follows. The mathematical model and formulations are introduced in Section 2. The two solution methods for the liquid-plate-coupled sloshing system are developed in Section 3. Extensive results are provided for different edge conditions in Section 4. Conclusions are given in Section 5.

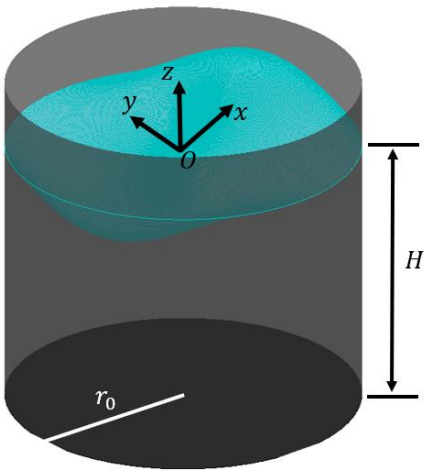

Fig. 1. Illustration of liquid sloshing in a cylindrical tank with elastic cover.

2. Mathematical model and formulations

We consider liquid sloshing in a circular cylindrical tank. The tank wall is assumed to be rigid, while an elastic cover is on the top surface of the fluid. Cartesian and cylindrical coordinate systems, or $Oxyz$ and $Or\theta z$ with $x = r\cos\theta$ and $y = r\sin\theta$, fixed on the tank are established, with their origins located on the mean upper surface of the fluid domain, and the z-axes pointing vertically upwards along the centre line of

the tank. The liquid is assumed to be inviscid and incompressible, and its motion is irrotational. Therefore, the velocity potential Φ can be adopted to describe the fluid motion. It satisfies the Laplace equation

$$\nabla^2\Phi + \frac{\partial^2\Phi}{\partial z^2} = \frac{\partial^2\Phi}{\partial x^2} + \frac{\partial^2\Phi}{\partial y^2} + \frac{\partial^2\Phi}{\partial z^2} = 0, \tag{1}$$

in the Cartesian system, which can be converted into the cylindrical system as

$$\frac{\partial^2\Phi}{\partial r^2} + \frac{1}{r}\frac{\partial\Phi}{\partial r} + \frac{1}{r^2}\frac{\partial^2\Phi}{\partial\theta^2} + \frac{\partial^2\Phi}{\partial z^2} = 0. \tag{2}$$

Here ∇^2 is the two-dimensional Laplacian operator. When the motion amplitude is small compared with the tank dimension and the typical wavelength of the sloshing motion, the boundary conditions can be linearized. In such a case, the deflection of elastic cover W and velocity potential Φ satisfy the following dynamic and kinematic conditions

$$\rho_e h\frac{\partial^2 W}{\partial t^2} + L\nabla^4 W = -\rho\Phi_t - \rho g W, \tag{3}$$

$$W_t = \Phi_z, \tag{4}$$

on the interface $z = 0$, where $L = Eh^3/[12(1-\nu^2)]$ is the flexural rigidity with E, h, ρ_e and ν being the Young's modulus, thickness, density and Poisson's ratio of the elastic plate, ρ is the density of the liquid and g is the acceleration due to gravity. The combination of Eqs.(3) and (4) gives

$$\left(L\nabla^4 + \rho_e h\frac{\partial^2}{\partial t^2} + \rho g\right)\Phi_z = -\rho\frac{\partial^2\Phi}{\partial t^2}, \qquad z = 0. \tag{5}$$

On the tank wall, the impermeable boundary condition gives

$$\left.\frac{\partial\Phi}{\partial r}\right|_{r=r_0} = 0, \tag{6}$$

while on the tank bottom

$$\left.\frac{\partial\Phi}{\partial z}\right|_{z=-H} = 0, \tag{7}$$

where r_0 is the radius of the tank and H is the depth of liquid.

In addition, the elastic cover is assumed to extend to the tank wall. We may consider three types of commonly used edge conditions (Timoshenko and Woinowsky-Krieger [21]), or clamped edge:

$$W|_{r=r_0} = 0, \qquad \left.\frac{\partial W}{\partial r}\right|_{r=r_0} = 0, \tag{8}$$

free edge:

$$\left.\begin{aligned} \nabla^2 W|_{r=r_0} &= \frac{1-\nu}{r_0}\left[\left(\frac{1}{r_0}\frac{\partial^2}{\partial\theta^2}+\frac{\partial}{\partial r}\right)W\right]_{r=r_0} \\ \left[\frac{\partial}{\partial r}\nabla^2 W\right]_{r=r_0} &= -\frac{1-\nu}{r_0^2}\left[\left(\frac{\partial^3}{\partial\theta^2\partial r}-\frac{1}{r_0}\frac{\partial^2}{\partial\theta^2}\right)W\right]_{r=r_0} \end{aligned}\right\}, \tag{9}$$

and simply supported edge:

$$\nabla^2 W|_{r=r_0} = \frac{1-\nu}{r_0}\left[\left(\frac{1}{r_0}\frac{\partial^2}{\partial\theta^2}+\frac{\partial}{\partial r}\right)W\right]_{r=r_0}, \qquad W|_{r=r_0} = 0. \tag{10}$$

3. Solution procedures for the natural frequencies

We consider the case in which the liquid is set into motion by some initial disturbance and will then continue oscillating on its own at its natural modes without further excitation. Assuming that ω is a natural frequency, we may write the velocity potential and the cover deflection as $\Phi(x,y,z,t) = \mathrm{Re}\{\phi(x,y,z)\times e^{-i\omega t}\}$ and $W(x,y,t) = \mathrm{Re}\{w(x,y)\times \mathrm{e}^{-i\omega t}\}$, respectively.

3.1 Solution using a Bessel-Fourier series expansion

The dynamic and kinematic conditions in Eqs. (3) and (4) can be written as

$$L\nabla^4 w + (\rho g - \rho_e h\omega^2)w = i\omega\rho\phi, \quad z = 0, \tag{11}$$

$$-i\omega w = \phi_z, \quad z = 0. \tag{12}$$

The velocity potential ϕ may be expanded into a Fourier series in θ direction. Through variable separation method in r and z directions, we may write

$$\phi = \sum_{n=0}^{\infty}\sum_{m=1}^{\infty} J_n(\alpha_{nm}r)\,(a_{nm}\cos n\theta + b_{nm}\sin n\theta)\frac{\cosh\alpha_{nm}(z+H)}{\cosh\alpha_{nm}H}, \tag{13}$$

where J_n is the Bessel function of the first kind. Equation (13) automatically satisfies Eqs. (2) and (7). To satisfy Eq. (6), $\alpha_{nm} r_0$ will be the solution of $J_n'(\alpha_{nm} r_0) = 0$, or zeros of the first-order derivative of the Bessel function. It should be noted that the derivative here is taken in the sense $J_n'(z) = \mathrm{d}J_n/\mathrm{d}z$.

The deflection of the elastic cover can be expanded as

$$w(r,\theta) = \sum_{n=0}^{\infty} w_n^{(c)}(r)\cos n\theta + w_n^{(s)}(r)\sin n\theta. \tag{14}$$

Here the procedures to solve the problems of $w_n^{(c)}$ and $w_n^{(s)}$ are identical. We therefore focus on the former and use w_n for $w_n^{(c)}$. Due to the orthogonality of trigonometric functions, Eqs. (11) and (12) can be written in terms of w_n as

$$L\left(\frac{\partial^2}{\partial r^2} + \frac{1}{r}\frac{\partial}{\partial r} - \frac{n^2}{r^2}\right)^2 w_n + (\rho g - \rho_e h\omega^2) w_n = i\omega\rho \sum_{m=1}^{\infty} a_{nm} J_n(\alpha_{nm} r), \tag{15}$$

$$-i\omega w_n(r) = \sum_{m=1}^{\infty} a_{nm}\, \alpha_{nm}\, J_n(\alpha_{nm} r)\, \tanh \alpha_{nm} H. \tag{16}$$

It may seem that we could expand $w_n(r)$ into a Bessel-Fourier series as we have done for ϕ in Eq. (13). However, as discussed in Ren et al. [22] on the rectangular channel problem, it can be problematic when spatial derivatives in Eq. (3) are applied to the expansion. Thus, in Ren et al. [22], the expansion is then applied to $W''''(y)$ in the transverse direction y of the channel, and the expansion of W is obtained through integration of W''''. The result therefore contains four additional coefficients which are determined through edge conditions of the cover at the channel wall.

Here when we have the expansion for $w_n(r)$, we shall not take direct derivatives with respect r to obtain $w_n^{(k)}$ for $k = 1,2,3,4$. Instead, we shall obtain the expansion of the first term on the left-hand side of Eq. (15) through the following procedure. We first write

$$L_n(r) = \left(\frac{\partial^2}{\partial r^2} + \frac{1}{r}\frac{\partial}{\partial r} - \frac{n^2}{r^2}\right) w_n(r), \tag{17}$$

and then consider the following integration

$$I_m = \int_0^{r_0} L_n \; r\, J_n(\alpha_{nm} r)\mathrm{d}r = \int_0^{r_0} \left(\frac{\partial^2}{\partial r^2} + \frac{1}{r}\frac{\partial}{\partial r} - \frac{n^2}{r^2}\right) w_n \; r\, J_n(\alpha_{nm} r)\mathrm{d}r. \qquad (18)$$

Through integration by parts, we obtain

$$\begin{aligned} I_m &= r_0 J_n(\alpha_{nm} r_0) w_n{}'(r_0) - r_0 \alpha_{nm} J_n'(\alpha_{nm} r_0) w_n(r_0) \\ &\quad + \int_0^{r_0} w_n \left\{ [r\, J_n(\alpha_{nm} r)]'' - [J_n(\alpha_{nm} r)]' - \frac{n^2}{r} J_n(\alpha_{nm} r) \right\} \mathrm{d}r \\ &= r_0\, J_n(\alpha_{nm} r_0) w_n{}'(r_0) - r_0 \alpha_{nm} J_n'(\alpha_{nm} r_0) w_n(r_0) \\ &\quad - \int_0^{r_0} \alpha_{nm}^2 \, w_n \, r\, J_n(\alpha_{nm} r)\, \mathrm{d}r \end{aligned} \qquad (19)$$

where Eq. (9.1.1) of Abramowitz and Stegun [23] or the differential equation satisfied by the Bessel function has been used. We then apply the procedure in Eq. (18) to the first term on the left-hand side of Eq. (15), or

$$M_n(r) = \left(\frac{\partial^2}{\partial r^2} + \frac{1}{r}\frac{\partial}{\partial r} - \frac{n^2}{r^2}\right) L_n = \left(\frac{\partial^2}{\partial r^2} + \frac{1}{r}\frac{\partial}{\partial r} - \frac{n^2}{r^2}\right)^2 w_n, \qquad (20)$$

and we have

$$\begin{aligned} K_m &= \int_0^{r_0} M_n \; r\, J_n(\alpha_{nm} r)\mathrm{d}r \\ &= r_0\, J_n(\alpha_{nm} r_0) \left.\frac{\partial L_n}{\partial r}\right|_{r=r_0} - r_0 \alpha_{nm} J_n'(\alpha_{nm} r_0) L_n|_{r=r_0} - \alpha_{nm}^2 I \\ &= r_0 \; J_n(\alpha_{nm} r_0) \left.\frac{\partial L_n}{\partial r}\right|_{r=r_0} - r_0 \alpha_{nm} \; J_n'(\alpha_{nm} r_0)\, L_n|_{r=r_0} \\ &\quad - r_0 \alpha_{nm}^2 \; J_n(\alpha_{nm} r_0) \left.\frac{\partial w_n}{\partial r}\right|_{r=r_0} + r_0 \alpha_{nm}^3 \; J_n'(\alpha_{nm} r_0)\, w_n|_{r=r_0} \\ &\quad + \alpha_{nm}^4 \int_0^{r_0} r\, J_n(\alpha_{nm} r)\, w_n \, \mathrm{d}r\,. \end{aligned} \qquad (21)$$

We now expand $w_n(r)$ as

$$w_n(r) = \sum_{m=1}^{\infty} e_m J_n(\alpha_{nm} r). \qquad (22)$$

Using the orthogonality of the Bessel function, and noticing $J_n'(\alpha_{nm} r_0) = 0$, Eqs. (19) and (21) give

$$I_m = r_0\, J_n(\alpha_{nm} r_0) \left.\frac{\partial w_n}{\partial r}\right|_{r=r_0} - \alpha_{nm}^2\, e_m\, \Omega_{nm}, \tag{23}$$

$$K_m = r_0\ J_n(\alpha_{nm} r_0) \left.\frac{\partial L_n}{\partial r}\right|_{r=r_0} - r_0 \alpha_{nm}^2\ J_n(\alpha_{nm} r_0) \left.\frac{\partial w_n}{\partial r}\right|_{r=r_0} + \alpha_{nm}^4\, e_m\, \Omega_{nm}, \tag{24}$$

where

$$\Omega_{nm} = \frac{(\alpha_{nm}^2 r_0^2 - n^2) J_n^2(\alpha_{nm} r_0)}{2\alpha_{nm}^2}. \tag{25}$$

Thus,

$$L_n(r) = \sum_{m=1}^{\infty} \frac{I_m}{\Omega_{nm}}\, J_n(\alpha_{nm} r), \tag{26}$$

$$M_n(r) = \sum_{m=1}^{\infty} \frac{K_m}{\Omega_{nm}}\, J_n(\alpha_{nm} r). \tag{27}$$

We may notice that these expansions are different from those obtained by substituting Eq. (22) directly into Eqs. (17) and (20).

Using Eqs. (13), (22) and (27) and the orthogonality of trigonometric and Bessel functions, from Eqs. (15) and (16) we can further have

$$LK_m + (\rho g - \rho_e h\omega^2) e_m \Omega_{nm} = i\omega\rho a_{nm}\, \Omega_{nm}, \tag{28}$$

$$-i\omega e_m = a_{nm}\, \alpha_{nm} \tanh \alpha_{nm} H. \tag{29}$$

Substituting Eqs. (24) and (29) into Eq. (28), we have

$$r_0\ J_n(\alpha_{nm} r_0) \left.\frac{\partial L_n}{\partial r}\right|_{r=r_0} - r_0 \alpha_{nm}^2\ J_n(\alpha_{nm} r_0) \left.\frac{\partial w_n}{\partial r}\right|_{r=r_0}$$
$$= \frac{e_m \Omega_{nm}}{L} \left[\frac{\rho\omega^2}{\alpha_{nm} \tanh \alpha_{nm} H} - (L\alpha_{nm}^4 + \rho g - \rho_e h\omega^2) \right]. \tag{30}$$

There are still edge conditions to be imposed. From Eq. (30), we can have

$$e_m = \frac{L\left(r_0\ J_n(\alpha_{nm} r_0) \left.\frac{\partial L_n}{\partial r}\right|_{r=r_0} - r_0 \alpha_{nm}^2\ J_n(\alpha_{nm} r_0) \left.\frac{\partial w_n}{\partial r}\right|_{r=r_0} \right)}{\left[\frac{\rho\omega^2}{\alpha_{nm} \tanh \alpha_{nm} H} - (L\alpha_{nm}^4 + \rho g - \rho_e h\omega^2) \right] \Omega_{nm}}. \tag{31}$$

The edge conditions, in Eqs. (8) to (10), can be given explicitly for w_n. For clamped edge,

$$w_n|_{r=r_0} = 0, \quad \left.\frac{\partial w_n}{\partial r}\right|_{r=r_0} = 0. \tag{32}$$

By using Eq. (17), the free and simply supported edge conditions in Eqs. (9) and (10) can be respectively written as

$$\left.\begin{aligned} [L_n(r)]_{r=r_0} &= \frac{1-\nu}{r_0}\left(\frac{\partial}{\partial r}w_n(r) - \frac{n^2}{r_0}w_n(r)\right)_{r=r_0} \\ \left[\frac{\partial}{\partial r}L_n\right]_{r=r_0} &= -\frac{1-\nu}{r_0^2}\left[\left(-n^2\frac{\partial}{\partial r} + \frac{n^2}{r_0}\right)w_n\right]_{r=r_0} \end{aligned}\right\}, \tag{33}$$

and

$$\left.\begin{aligned} [L_n(r)]_{r=r_0} &= \frac{1-\nu}{r_0}\left(\frac{\partial}{\partial r}w_n(r) - \frac{n^2}{r_0}w_n(r)\right)_{r=r_0} \\ w_n|_{r=r_0} &= 0 \end{aligned}\right\}. \tag{34}$$

Substituting Eqs. (22), (23), (26) and (31) into one of the above sets of edge conditions Eqs. (32) to (34), we can have

$$\left.\begin{aligned} \left.\frac{\partial L_n}{\partial r}\right|_{r=r_0} \times A_{11} + \left.\frac{\partial w_n}{\partial r}\right|_{r=r_0} \times A_{12} &= 0 \\ \left.\frac{\partial L_n}{\partial r}\right|_{r=r_0} \times A_{21} + \left.\frac{\partial w_n}{\partial r}\right|_{r=r_0} \times A_{22} &= 0 \end{aligned}\right\} \tag{35}$$

where

$$\left.\begin{aligned} A_{11} &= \sum_{m=1}^{\infty} \frac{2\alpha_{nm}^2 L r_0}{\left[\frac{\rho\omega^2}{\alpha_{nm}\tanh\alpha_{nm}H} - (L\alpha_{nm}^4 + \rho g - \rho_e h\omega^2)\right](\alpha_{nm}^2 r_0^2 - n^2)} \\ A_{12} &= -\sum_{m=1}^{\infty} \frac{2\alpha_{nm}^4 L r_0}{\left[\frac{\rho\omega^2}{\alpha_{nm}\tanh\alpha_{nm}H} - (L\alpha_{nm}^4 + \rho g - \rho_e h\omega^2)\right](\alpha_{nm}^2 r_0^2 - n^2)} \\ A_{21} &= 0 \\ A_{22} &= 1 \end{aligned}\right\} \tag{36}$$

for the clamped edges,

$$\left.\begin{aligned}
A_{11} &= -\sum_{m=1}^{\infty} \frac{2\alpha_{nm}^2 L r_0 \left(\alpha_{nm}^2 - \frac{(1-\nu)n^2}{r_0^2}\right)}{\left[\frac{\rho\omega^2}{\alpha_{nm}\tanh\alpha_{nm}H} - (L\alpha_{nm}^4 + \rho g - \rho_e h\omega^2)\right](\alpha_{nm}^2 r_0^2 - n^2)} \\
A_{12} &= -\frac{1-\nu}{r_0} + \sum_{m=1}^{\infty} \frac{2\alpha_{nm}^2 r_0 \left[\frac{\rho\omega^2}{\alpha_{nm}\tanh\alpha_{nm}H} - (\rho g - \rho_e h\omega^2) - L\alpha_{nm}^2 \frac{(1-\nu)n^2}{r_0^2}\right]}{\left[\frac{\rho\omega^2}{\alpha_{nm}\tanh\alpha_{nm}H} - (L\alpha_{nm}^4 + \rho g - \rho_e h\omega^2)\right](\alpha_{nm}^2 r_0^2 - n^2)} \\
A_{21} &= 1 + \frac{(1-\nu)n^2}{r_0^2} \sum_{m=1}^{\infty} \frac{2\alpha_{nm}^2 L}{\left[\frac{\rho\omega^2}{\alpha_{nm}\tanh\alpha_{nm}H} - (L\alpha_{nm}^4 + \rho g - \rho_e h\omega^2)\right](\alpha_{nm}^2 r_0^2 - n^2)} \\
A_{22} &= -\frac{(1-\nu)n^2}{r_0^2}\left\{1 + \sum_{m=1}^{\infty} \frac{2\alpha_{nm}^4 L}{\left[\frac{\rho\omega^2}{\alpha_{nm}\tanh\alpha_{nm}H} - (L\alpha_{nm}^4 + \rho g - \rho_e h\omega^2)\right](\alpha_{nm}^2 r_0^2 - n^2)}\right\}
\end{aligned}\right\} \quad (37)$$

for the free edges and

$$\left.\begin{aligned}
A_{11} &= -\sum_{m=1}^{\infty} \frac{2\alpha_{nm}^2 L r_0 \left(\alpha_{nm}^2 - \frac{(1-\nu)n^2}{r_0^2}\right)}{\left[\frac{\rho\omega^2}{\alpha_{nm}\tanh\alpha_{nm}H} - (L\alpha_{nm}^4 + \rho g - \rho_e h\omega^2)\right](\alpha_{nm}^2 r_0^2 - n^2)} \\
A_{12} &= -\frac{1-\nu}{r_0} + \sum_{m=1}^{\infty} \frac{2\alpha_{nm}^2 r_0 \left[\frac{\rho\omega^2}{\alpha_{nm}\tanh\alpha_{nm}H} - (\rho g - \rho_e h\omega^2) - L\alpha_{nm}^2 \frac{(1-\nu)n^2}{r_0^2}\right]}{\left[\frac{\rho\omega^2}{\alpha_{nm}\tanh\alpha_{nm}H} - (L\alpha_{nm}^4 + \rho g - \rho_e h\omega^2)\right](\alpha_{nm}^2 r_0^2 - n^2)} \\
A_{21} &= \sum_{m=1}^{\infty} \frac{2Lr_0\alpha_{nm}^2}{\left[\frac{\rho\omega^2}{\alpha_{nm}\tanh\alpha_{nm}H} - (L\alpha_{nm}^4 + \rho g - \rho_e h\omega^2)\right](\alpha_{nm}^2 r_0^2 - n^2)} \\
A_{22} &= -\sum_{m=1}^{\infty} \frac{2Lr_0\alpha_{nm}^4}{\left[\frac{\rho\omega^2}{\alpha_{nm}\tanh\alpha_{nm}H} - (L\alpha_{nm}^4 + \rho g - \rho_e h\omega^2)\right](\alpha_{nm}^2 r_0^2 - n^2)}
\end{aligned}\right\} \quad (38)$$

for the simply supported edges.

Therefore, the natural frequencies can be obtained from $A_{11}A_{22} - A_{21}A_{12} = 0$. For clamped edge, A_{21} and A_{22} in Eq. (36) are obtained by first differentiating Eq. (22) and then working out the summation explicitly as $r \to r_0$, together with Eq. (31). As a result, Eq. (35) is the same as that when taking $\left.\frac{\partial w_n}{\partial r}\right|_{r=r_0} = 0$ in Eq. (31) and then imposing only $w_n(r_0) = 0$ on Eq. (22). Because of this, the equation for the natural frequencies in the clamped edge case simply becomes $A_{11} = 0$, or

$$\sum_{m=1}^{\infty} \frac{2Lr_0\alpha_{nm}^2}{\left[\frac{\rho\omega^2}{\alpha_{nm}\tanh\alpha_{nm}H} - (L\alpha_{nm}^4 + \rho g - \rho_e h\omega^2)\right](\alpha_{nm}^2 r_0^2 - n^2)} = 0. \quad (39)$$

3.2 Solution using the vertical mode expansion

Based on separation of variables, the velocity potential can be also expanded as the following form

$$\phi = \sum_{m=-2}^{\infty} \varphi_m(r,\theta)\cdot\psi_m(z), \quad (40)$$

where

$$\varphi_m(r,\theta) = \sum_{n=0}^{\infty} \frac{J_n(\kappa_m r)}{J_n(\kappa_m r_0)}[a_{mn}\cos n\theta + b_{mn}\sin n\theta], \quad (41)$$

$$\psi_m(z) = \frac{\cosh\kappa_m(z+H)}{\cosh\kappa_m H}. \quad (42)$$

κ_m are eigenvalues and can be obtained from the dispersion relation corresponding to the boundary condition in Eq. (5):

$$(L\kappa_m^4 + \rho g - \rho_e h\omega^2)\kappa_m \sinh\kappa_m H - \rho\omega^2\cosh\kappa_m H = 0. \quad (43)$$

κ_{-2}, κ_{-1} are the complex roots with positive imaginary part, κ_0 as the positive real root, and κ_n $(n = 1,2,3\ldots)$ are the positive pure imaginary roots.

The orthogonal inner product defined in Sahoo et al. [24] is given as

$$\langle\psi_m,\psi_{\tilde{m}}\rangle = \int_{-H}^{0} \psi_m\,\psi_{\tilde{m}}\,\mathrm{d}z + \frac{L}{\rho\omega^2}\left[\frac{\partial\psi_m}{\partial z}\frac{\mathrm{d}^3\psi_{\tilde{m}}}{\mathrm{d}z^3} + \frac{\partial^3\psi_m}{\partial z^3}\frac{\mathrm{d}\psi_{\tilde{m}}}{\mathrm{d}z}\right]_{z=0} = S_m\,\delta_{m\tilde{m}} \quad (44)$$

where δ_{ij} is the Kronecker delta function and

$$S_m = \frac{2\kappa_m H + \sinh 2\kappa_m H}{4\kappa_m\cosh^2\kappa_m H} + \frac{2L\kappa_m^4}{\rho\omega^2}\tanh^2\kappa_m H. \quad (45)$$

Therefore,

$$\langle\frac{\partial\phi}{\partial r},\psi_{\tilde{m}}\rangle=\int_{-H}^{0}\frac{\partial\phi}{\partial r}\psi_{\tilde{m}}\,\mathrm{d}z+\frac{L}{\rho\omega^2}\left[\frac{\partial^2\phi}{\partial z\partial r}\frac{\mathrm{d}^3\psi_{\tilde{m}}}{\mathrm{d}z^3}+\frac{\partial^4\phi}{\partial z^3\partial r}\frac{\mathrm{d}\psi_{\tilde{m}}}{\mathrm{d}z}\right]_{z=0}=\frac{\partial\varphi_{\tilde{m}}}{\partial r}S_{\tilde{m}}. \quad (46)$$

On the tank wall, the impermeable condition Eq. (6) gives

$$\frac{\partial\phi}{\partial r}=0, \qquad (r=r_0). \quad (47)$$

Substitution of Eq. (47) into Eq. (46) gives

$$\frac{L}{\rho\omega^2}\left[\frac{\partial^2\phi}{\partial z\partial r}\frac{\mathrm{d}^3\psi_{\tilde{m}}}{\mathrm{d}z^3}+\frac{\partial^4\phi}{\partial z^3\partial r}\frac{\mathrm{d}\psi_{\tilde{m}}}{\mathrm{d}z}\right]_{r=r_0,\,z=0}=\left.\frac{\partial\varphi_{\tilde{m}}}{\partial r}\right|_{r=r_0}S_{\tilde{m}}. \quad (48)$$

We let

$$\beta(\theta)=\left.\frac{\partial^2\phi}{\partial z\partial r}\right|_{r=r_0,z=0}=\sum_{n=0}^{\infty}(e_n\cos n\theta+f_n\sin n\theta), \quad (49)$$

$$\gamma(\theta)=\left.\frac{\partial^4\phi}{\partial z^3\partial r}\right|_{r=r_0,z=0}=\sum_{n=0}^{\infty}(c_n\cos n\theta+d_n\sin n\theta). \quad (50)$$

Similar to Eq. (14), as the procedures for the problems in terms of $\cos n\theta$ and $\sin n\theta$ are identical, we consider only the cases of $\cos n\theta$ in the following analysis. Substituting Eqs. (40), (41), (42), (49) and (50) into Eq. (48), and using the orthogonality of trigonometric functions, we obtain

$$a_{mn}=\frac{L\tanh\kappa_m H}{\rho\omega^2\kappa_m S_m}\times\frac{J_n(\kappa_m r_0)}{J_n'(\kappa_m r_0)}\times(e_n\kappa_m^3+c_n\kappa_m), \quad (51)$$

Substituting Eqs. (40)~(42) and (51) into one of the edge conditions in Eqs. (32) to (34) and noticing $w=\partial\phi/\partial z$, we have

$$\left.\begin{aligned}c_nA_{11}^{(n)}+e_nA_{12}^{(n)}=0\\ c_nA_{21}^{(n)}+e_nA_{22}^{(n)}=0\end{aligned}\right\} \quad n=0,1,2,3\ldots \quad (52)$$

where

$$\left.\begin{aligned} A_{11}^{(n)} &= \sum_{m=-2}^{\infty} \frac{L\kappa_m \tanh^2 \kappa_m H}{\rho\omega^2 S_m} \times \frac{J_n(\kappa_m r_0)}{J_n'(\kappa_m r_0)} \\ A_{12}^{(n)} &= \sum_{m=-2}^{\infty} \frac{L\kappa_m^3 \tanh^2 \kappa_m H}{\rho\omega^2 S_m} \times \frac{J_n(\kappa_m r_0)}{J_n'(\kappa_m r_0)} \\ A_{21}^{(n)} &= \sum_{m=-2}^{\infty} \frac{L\kappa_m^2 \tanh^2 \kappa_m H}{\rho\omega^2 S_m} \\ A_{22}^{(n)} &= \sum_{m=-2}^{\infty} \frac{L\kappa_m^4 \tanh^2 \kappa_m H}{\rho\omega^2 S_m} \end{aligned}\right\} \tag{53}$$

for the clamped edge,

$$\left.\begin{aligned} A_{11}^{(n)} &= \sum_{m=-2}^{\infty} \frac{L\kappa_m \tanh^2 \kappa_m H}{\rho\omega^2 S_m} \times \frac{J_n(\kappa_m r_0)}{J_n'(\kappa_m r_0)} \times \left(-\kappa_m^2 + \frac{(1-\nu)n^2}{r_0^2} - \frac{(1-\nu)}{r_0} \frac{J_n'(\kappa_m r_0)}{J_n(\kappa_m r_0)} \kappa_m \right) \\ A_{12}^{(n)} &= \sum_{m=-2}^{\infty} \frac{L\kappa_m^3 \tanh^2 \kappa_m H}{\rho\omega^2 S_m} \times \frac{J_n(\kappa_m r_0)}{J_n'(\kappa_m r_0)} \times \left(-\kappa_m^2 + \frac{(1-\nu)n^2}{r_0^2} - \frac{(1-\nu)}{r_0} \frac{J_n'(\kappa_m r_0)}{J_n(\kappa_m r_0)} \kappa_m \right) \\ A_{21}^{(n)} &= \sum_{m=-2}^{\infty} \frac{L\kappa_m \tanh^2 \kappa_m H}{\rho\omega^2 S_m} \times \frac{J_n(\kappa_m r_0)}{J_n'(\kappa_m r_0)} \times \left(\frac{(1-\nu)n^2}{r_0^3} - \frac{J_n'(\kappa_m r_0)}{J_n(\kappa_m r_0)} \left(\kappa_m^3 + \frac{(1-\nu)n^2}{r_0^2} \kappa_m \right) \right) \\ A_{22}^{(n)} &= \sum_{m=-2}^{\infty} \frac{L\kappa_m^3 \tanh^2 \kappa_m H}{\rho\omega^2 S_m} \times \frac{J_n(\kappa_m r_0)}{J_n'(\kappa_m r_0)} \times \left(\frac{(1-\nu)n^2}{r_0^3} - \frac{J_n'(\kappa_m r_0)}{J_n(\kappa_m r_0)} \left(\kappa_m^3 + \frac{(1-\nu)n^2}{r_0^2} \kappa_m \right) \right) \end{aligned}\right\} \tag{54}$$

for the free edge, and

$$\left.\begin{aligned} A_{11}^{(n)} &= \sum_{m=-2}^{\infty} \frac{L\kappa_m \tanh^2 \kappa_m H}{\rho\omega^2 S_m} \times \frac{J_n(\kappa_m r_0)}{J_n'(\kappa_m r_0)} \times \left(-\kappa_m^2 + \frac{(1-\nu)n^2}{r_0^2} - \frac{(1-\nu)}{r_0} \frac{J_n'(\kappa_m r_0)}{J_n(\kappa_m r_0)} \kappa_m \right) \\ A_{12}^{(n)} &= \sum_{m=-2}^{\infty} \frac{L\kappa_m^3 \tanh^2 \kappa_m H}{\rho\omega^2 S_m} \times \frac{J_n(\kappa_m r_0)}{J_n'(\kappa_m r_0)} \times \left(-\kappa_m^2 + \frac{(1-\nu)n^2}{r_0^2} - \frac{(1-\nu)}{r_0} \frac{J_n'(\kappa_m r_0)}{J_n(\kappa_m r_0)} \kappa_m \right) \\ A_{21}^{(n)} &= \sum_{m=-2}^{\infty} \frac{L\kappa_m \tanh^2 \kappa_m H}{\rho\omega^2 S_m} \times \frac{J_n(\kappa_m r_0)}{J_n'(\kappa_m r_0)} \\ A_{22}^{(n)} &= \sum_{m=-2}^{\infty} \frac{L\kappa_m^3 \tanh^2 \kappa_m H}{\rho\omega^2 S_m} \times \frac{J_n(\kappa_m r_0)}{J_n'(\kappa_m r_0)} \end{aligned}\right\} \tag{55}$$

for the simply supported edge.

For non-trivial solution, we should have $A_{11}^{(n)}A_{22}^{(n)} - A_{12}^{(n)}A_{21}^{(n)} = 0$, which gives the natural frequencies. For the clamped edge specifically, by using the identities (A4) and (A5) in Evans and Porter [25], we can obtain

$$A_{21}^{(n)} = \frac{L}{\rho\omega^2}\sum_{m=-2}^{\infty}\frac{\tanh^2\kappa_m H\cdot\kappa_m^2}{S_m} = 0, \qquad A_{22}^{(n)} = \frac{L}{\rho\omega^2}\sum_{m=-2}^{\infty}\frac{\tanh^2\kappa_m H\cdot\kappa_m^4}{S_m} = 1.$$

Therefore, the formula for the natural frequencies can be further simplified as

$$\sum_{m=-2}^{\infty}\frac{\kappa_m\tanh^2\kappa_m H}{S_m}\times\frac{J_n(\kappa_m r_0)}{J_n'(\kappa_m r_0)} = 0. \tag{56}$$

Eq. (56) may seem very different form Eq. (39) for the same problem. However, it can be shown that they are in fact identical. We may define

$$K(\omega,\alpha) = (L\alpha^4 + \rho g - \rho_e h\omega^2)\alpha\sinh\alpha H - \rho\omega^2\cosh\alpha H, \tag{57}$$

and at $\alpha = \kappa_m$ it becomes Eq. (43). We have

$$\begin{aligned}\frac{\partial K}{\partial\alpha}(\alpha=\kappa_m) &= K'(\omega,\kappa_m)\\ &= (4L\kappa_m^4 - \rho\omega^2 H)\sinh\kappa_m H\\ &+ (L\kappa_m^4 + \rho g - \rho_e h\omega^2)(\sinh\kappa_m H + \kappa_m H\cosh\kappa_m H),\end{aligned} \tag{58}$$

or,

$$K'(\omega,\kappa_m) = 2\rho\omega^2\frac{\cosh^2\kappa_m H}{\sinh\kappa_m H}\times S_m. \tag{59}$$

We further construct a function as

$$f(\alpha) = \frac{\alpha\sinh\alpha H}{K(\omega,\alpha)}\times\frac{J_n(\alpha r_0)}{J_n'(\alpha r_0)}. \tag{60}$$

Integrating $f(\alpha)$ along a circle of infinite radius R centred at the origin in the complex plane, and using residual theorem at $K(\omega,\kappa_m) = 0$ and $J_n'(\alpha_{nm}r_0) = 0$, we have

$$I_1 = \frac{1}{2\pi i}\oint_c f(\alpha)\,\mathrm{d}\alpha$$
$$= 2\left(\sum_{m=-2}^{\infty}\frac{\kappa_m \sinh\kappa_m H}{K'(\omega,\kappa_m)}\times\frac{J_n(\kappa_m r_0)}{J_n'(\kappa_m r_0)} + \sum_{m=1}^{\infty}\frac{\alpha_{nm}\sinh\alpha_{nm}H}{K(\omega,\alpha_{nm})}\times\frac{J_n(\alpha_{nm}r_0)}{r_0 J_n''(\alpha_{nm}r_0)}\right). \quad (61)$$

When $R \to \infty$, $I_1 \to 0$. Also, from Eq. (56), the first series on the right-hand side of Eq. (61) is

$$\sum_{m=-2}^{\infty}\frac{\kappa_m \sinh\kappa_m H}{K'(\omega,\kappa_m)}\times\frac{J_n(\kappa_m r_0)}{J_n'(\kappa_m r_0)} = \frac{1}{2\rho\omega^2}\sum_{m=-2}^{\infty}\frac{\kappa_m \tanh^2\kappa_m H}{S_m}\times\frac{J_n(\kappa_m r_0)}{J_n'(\kappa_m r_0)} = 0. \quad (62)$$

Thus, we have

$$\sum_{m=1}^{\infty}\frac{\alpha_{nm}\sinh\alpha_{nm}H}{K(\omega,\alpha_{nm})}\times\frac{J_n(\alpha_{nm}r_0)}{J_n''(\alpha_{nm}r_0)} = 0. \quad (63)$$

Furthermore, $J_n(\alpha_{nm}r_0)/J_n''(\alpha_{nm}r_0)$ in Eq. (63) can be simplified by using the differential equation satisfied by the Bessel function together with $J_n'(\alpha_{nm}r_0) = 0$,

$$\frac{J_n(\alpha_{nm}r_0)}{J_n''(\alpha_{nm}r_0)} = \frac{\alpha_{nm}^2 r_0^2}{n^2 - \alpha_{nm}^2 r_0^2}. \quad (64)$$

Equation (63) can be further written as

$$\sum_{m=1}^{\infty}\frac{\alpha_{nm}^2 r_0^2}{\left(L\alpha_{nm}^4 + \rho g - \rho_e h\omega^2 - \frac{\rho\omega^2}{\alpha_{nm}\tanh\alpha_{nm}H}\right)(n^2 - \alpha_{nm}^2 r_0^2)} = 0, \quad (65)$$

which is identical to Eq. (39).

4. Results and Analysis

4.1 Special case

Here we first consider a limit case with zero liquid density. When $\rho = 0$, the solution for the clamped edge can be simplified to

$$\sum_{m=1}^{\infty}\frac{1}{(L\alpha_{nm}^4 - \rho_e h\omega^2)}\times\frac{J_n(\alpha_{nm}r_0)}{J_n''(\alpha_{nm}r_0)} = 0. \quad (66)$$

Let $f(\alpha)=\frac{J_n(\alpha r_0)}{(L\alpha^4-\rho_e h\omega^2)\times J_n'(\alpha r_0)}$, and use residual theorem at $L\alpha_{nm}^4-\rho_e h\omega^2=0$ and $J_n'(\alpha_{nm}r_0)=0$, we can have

$$\sum_{m=1}^{4}\frac{1}{4L\lambda_{nm}^3}\times\frac{J_n(\lambda_{nm}r_0)}{J_n'(\lambda_{nm}r_0)}+2\sum_{m=1}^{\infty}\frac{1}{(L\alpha_{nm}^4-\rho_e h\omega^2)}\times\frac{J_n(\alpha_{nm}r_0)}{J_n''(\alpha_{nm}r_0)}=0. \tag{67}$$

From Eq. (66), we have

$$\sum_{m=1}^{4}\frac{1}{4L\lambda_{nm}^3}\times\frac{J_n(\lambda_{nm}r_0)}{J_n'(\lambda_{nm}r_0)}=0, \tag{68}$$

where $\lambda_{nm}^4=\frac{\rho_e h}{L}\omega^2$, or $\lambda_{n1}=-\lambda_{n2}=i\lambda_{n3}=-i\lambda_{n4}=ik$ with $k=\left(\frac{\rho_e h}{L}\omega^2\right)^{\frac{1}{4}}$. Equation (68) further gives

$$I_n(kr_0)J_n'(kr_0)+J_n(kr_0)I_n'(kr_0)=0. \tag{69}$$

where I_n is the modified Bessel function of the first kind. Similarly, by using residual theorem to infinite series in each A_{ij} in Eq. (38), we finally have

$$J_{n+1}(kr_0)I_n(kr_0)+I_{n+1}(kr_0)J_n(kr_0)=\frac{2kr_0}{1-\nu}\times J_n(kr_0)I_n(kr_0) \tag{70}$$

for the natural frequencies of simply supported plate in vacuum. These formulations are virtually the same as those provided by Wah [26] without tension. For the free edge case, by applying the residual theorem to infinite series in each A_{ij} of Eq. (37), we have

$$\begin{aligned}\frac{1-\nu}{kr_0}=&\left[\frac{(1-\nu)n^2}{k^2r_0^2}-\frac{(1-\nu)^2(n^4-n^2)}{2k^4r_0^4}-\frac{1}{2}\right]\times\frac{J_n(kr_0)}{J_n'(kr_0)}\\&+\left[\frac{(1-\nu)n^2}{k^2r_0^2}+\frac{(1-\nu)^2(n^4-n^2)}{2k^4r_0^4}+\frac{1}{2}\right]\times\frac{I_n(kr_0)}{I_n'(kr_0)}\\&-\frac{(1-\nu)n^2}{k^3r_0^3}\times\frac{J_n(kr_0)}{J_n'(kr_0)}\times\frac{I_n(kr_0)}{I_n'(kr_0)}.\end{aligned} \tag{71}$$

which is equivalent to the equation provided by Bauer [17].

4.2 Natural frequencies

In the analysis below, all the variables are non-dimensionalized based on the following three basic parameters, namely, the acceleration due to gravity g, the density of the liquid ρ as well as the radius of the tank r_0. Accordingly, the dimensionless parameters for the liquid depth H, the mass per unit area of the cover $\rho_e h$, and the flexural elasticity

L are $H^* = H/r_0$, $m^* = \rho_e h/(\rho r_0)$ and $L^* = L/(\rho g r_0^4)$, respectively. Similarly, the natural frequency ω can be non-dimensionalized as $\omega^* = \omega\sqrt{r_0/g}$. The Poisson's ratio ν is set as 0.3. Here the first method in Section 3.1 has been adopted for the calculation of the natural frequencies, and the second method is used for verification.

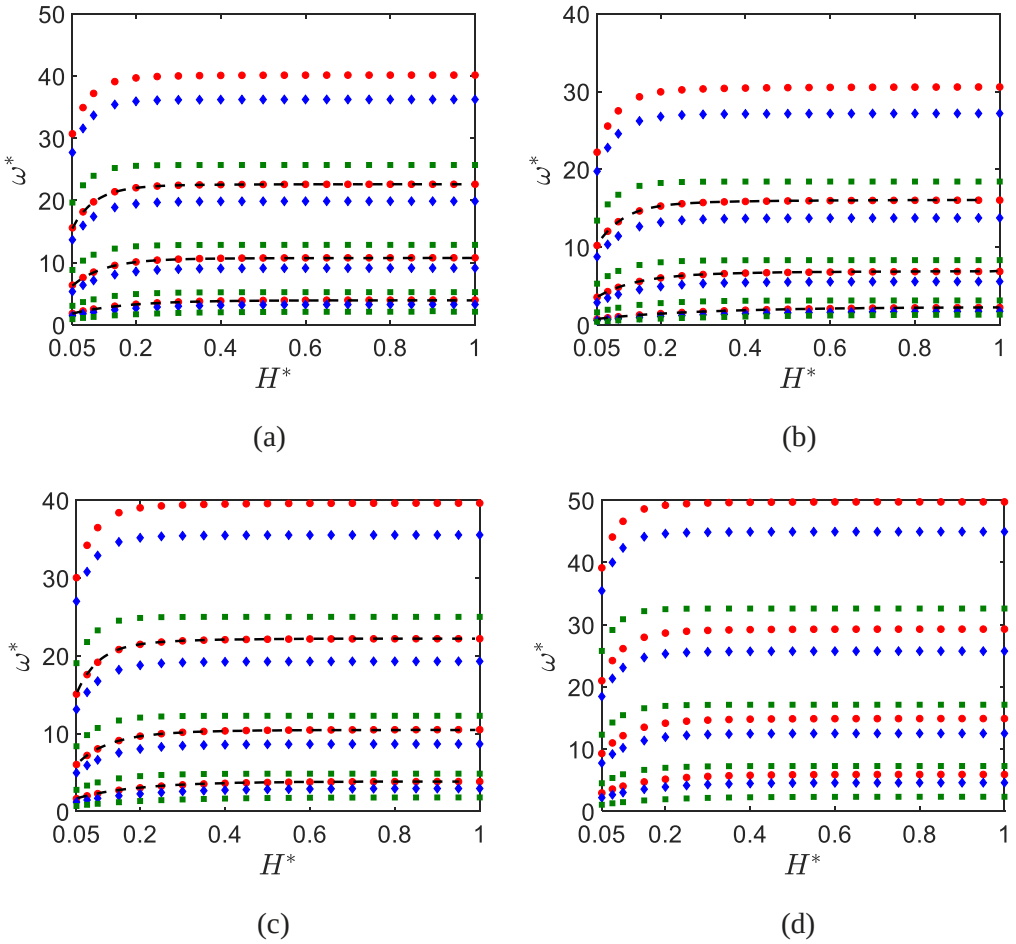

Fig. 2. The first four natural frequencies against different H^* for various edge conditions for $L^* = 2 \times 10^{-3}, m^* = 1 \times 10^{-3}$: (a) $n = 0$; (b) $n = 1$; (c) $n = 2$; (d) $n = 3$. clamped edge: red circles; simply supported edge: blue diamonds; free edge: green squares. Results from Bauer [17] for clamped edge are nondimensionalized and shown as black dashed lines for comparison in (a), (b) and (c).

We first investigate the effect of the liquid depth on the natural frequencies. For given m^* and L^*, we display the curves of ω^* against different H^* for various edge types in Fig. 2. The results for the clamped edge by Bauer [17] are provided for comparison in Fig. 2 (a, b, c), and good agreement can be found. For the kth natural frequencies, at a given H^*, the clamped edge corresponds to the largest value while the free edge corresponds to the smallest, which is consistent with the observation in Ren et al. [22]. In addition, with the increase of H^*, the curves increase rapidly to the limit values. This

could be understood through the term $\tanh \alpha_{nm}H$ in the denominators of Eqs. (36) to (38). With the increase of H, the value of $\tanh \alpha_{nm}H$ increases very rapidly and approaches to one when $H \to \infty$. Therefore, when liquid depth has reached a critical value, which makes $\tanh \alpha_{nm}H \to 1$ even for the smallest α_{nm}, the corresponding natural frequencies will not change very much with further increase of liquid depth.

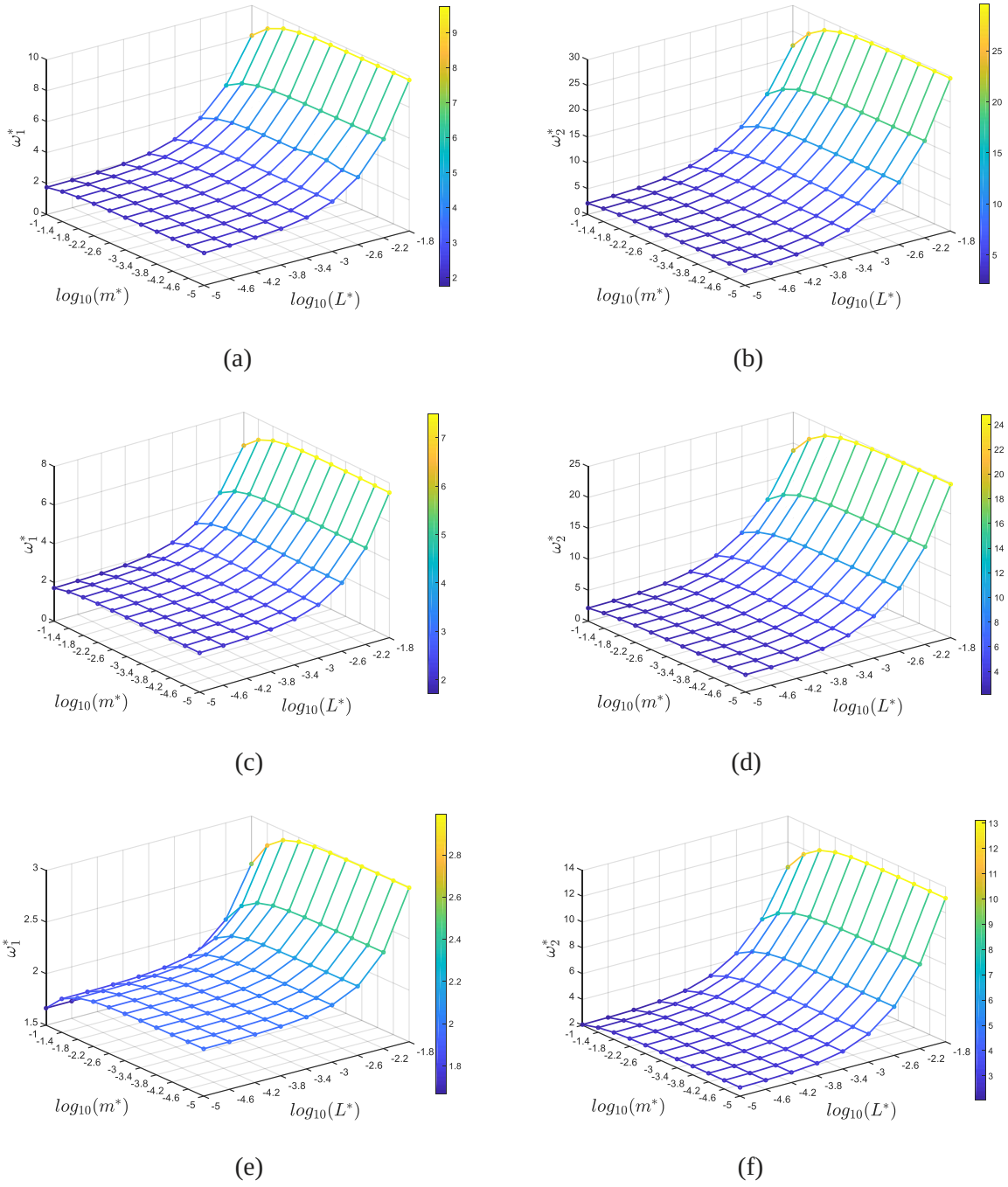

Fig. 3. Natural frequencies ω_k^* $(k = 1,2)$ against different L^* and m^* for various edge conditions for $H^* = 1$ at $n = 0$. (a) clamped edge for $k = 1$; (b) clamped edge for $k = 2$; (c) simply supported edge for $k = 1$; (d) simply supported edge for $k = 2$; (e) free edge for $k = 1$; (f) free edge for $k = 2$.

We further investigate the effect of L^* and m^* on the natural frequencies for a given H^*. For $n = 0$, the graphs for the first two natural frequencies against different pairs of L^* and m^* at different edge conditions are plotted in Fig. 3. In the figure, the logarithm base 10 of L^* and m^* are set as coordinates. We can observe that a similar variation trend of ω_k^* with L^* and m^* for all these three edge constraints. The natural frequencies ω_k^* will increase with the increasing of L^* or the decreasing of m^*. As the former is in fact the stiffness term and the latter is the mass term, the result is expected. However, it ought to point out that for the free surface problem without the elastic cover, the restoring force of the wave motion is also related to the density of the fluid and therefore the natural frequencies of the sloshing motion are independent to the density. Here when the physical properties of the elastic cover are given, L^* and m^* will be very much affected by the fluid density, or the natural frequencies of the fluid motion will be affected by its density. In practice, containers with same geometry may be used to store different liquids, for example, crude oil and LNG. For a fixed elastic cover, the change of liquid density leads to the changes of m^* and L^* simultaneously at a same rate. An increasing ρ corresponds to decreasing (L^*, m^*). In this case, it may be interesting to investigate the effect of liquid density on the natural frequencies. To do so, we may compare the natural frequencies corresponding to three pairs of (L^*, m^*) in Table 1. The results correspond to three separate points located in each graph of Fig. 3. Through comparing, we may find that the natural frequencies will increase with the increase of (L^*, m^*), or the decrease of ρ. This to some extent illustrates that changing L^* makes bigger difference to the natural frequencies than changing m^*. As discussed above, for the limit case where $\rho = 0$, ω_k^* can be obtained from Eqs. (69) to (71). When we consider the limit case where the liquid density is very large, or $\rho \to \infty$, both L^* and $m^* \to 0$, then it is identical to the case without the elastic cover. Therefore, the natural frequencies in this case will tend to that with free surface.

Table 1. Natural frequencies ω_k^* at different (L^*, m^*) at $n = 0$ and $H^* = 1$.

edge types, k / (L^*, m^*)	clamped $k = 1$	clamped $k = 2$	simply supported $k = 1$	simply supported $k = 2$	free $k = 1$	free $k = 2$
$(1 \times 10^{-3}, 5 \times 10^{-4})$	3.2155	7.8965	2.7495	6.7560	2.0514	4.1831
$(2 \times 10^{-3}, 1 \times 10^{-3})$	4.0008	10.7930	3.2885	9.1397	2.1274	5.2713
$(4 \times 10^{-3}, 2 \times 10^{-3})$	5.2202	14.9506	4.1558	12.5892	2.2683	6.9392

4.3 Shapes of natural modes

We also investigate the shapes of the natural modes at natural frequencies. As in Ren et al. [22], once the natural frequency ω_k^* $(k = 1,2, \dots)$ is obtained through solving the non-trivial solution, then we can prescribe one of the non-zero coefficients and calculate the rest through solving the system of linear equations. Here we notice that because of the orthogonality of the trigonometric functions, the natural modes at different n are independent to each other. At each n, we have two unknowns, $\frac{\partial L_n}{\partial r}\Big|_{r=r_0}$ and $\frac{\partial w_n}{\partial r}\Big|_{r=r_0}$. We can set one of them as unit and find the other from Eq. (35). In the results below, $\frac{\partial L_n}{\partial r}\Big|_{r=r_0} = 1$ is taken apart from the free edge case when $n = 0$ as it is zero from the boundary condition. In that particular case $\frac{\partial w_n}{\partial r}\Big|_{r=r_0} = 1$ is taken. e_m can be obtained from Eq. (31) and subsequently the shapes of natural modes can be found. For $n = 0$, it corresponds to an axisymmetric case, for which the first four modes are shown in Fig. 4 for various edge constraints. In the figure, we can observe that the peaks of the deflections at all modes occur at the centre of the cover, or $r^* = 0$. At the edge, w_0 are zero for clamped and simply supported cases due to the edge conditions. For free edge, the values of w_0 at the edge are non-zero but the amplitudes are smaller than those at the centre. The mode shapes become more oscillatory along the axial direction as the natural frequency increases. At higher ω, the acceleration of the deflection will be higher, which leads to a higher internal force and moment. This means larger spatial derivatives of the deflection or a faster spatial variation of the deflection, leading to a more oscillatory curve of $w_n(r)$.

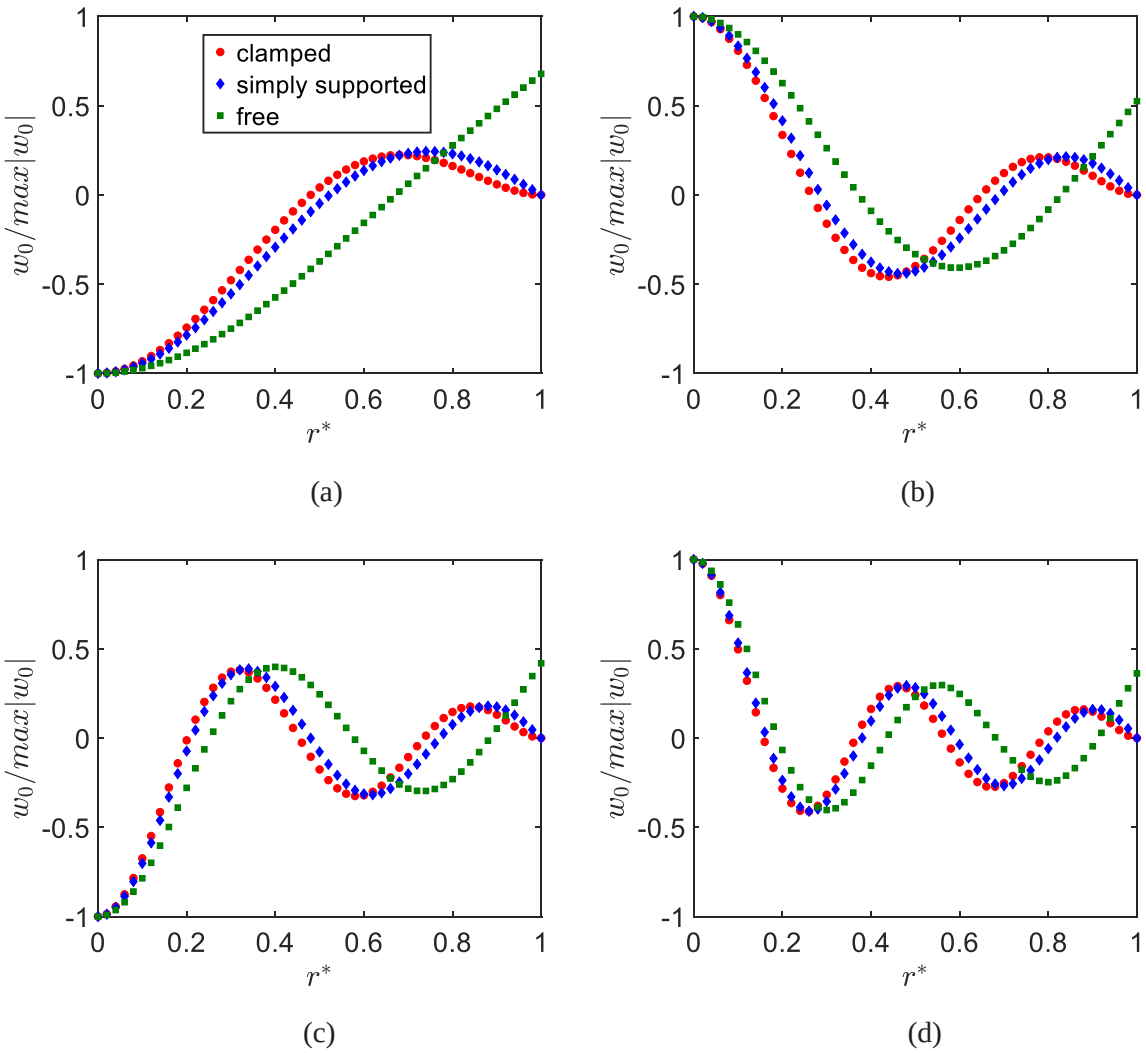

Fig. 4. Normalized mode shapes corresponding to $n = 0$ for various edge conditions at the k^{th} natural frequency ω_k^* (k = 1,2,3,4) with $H^* = 1, L^* = 2 \times 10^{-3}, m^* = 1 \times 10^{-3}$. (a). ω_1^*; (b). ω_2^*. (c). ω_3^*; (d). ω_4^*.

For $n > 0$, the mode shapes become non-axisymmetric. However, noticing that $J_n(0) = 0$ for all $n > 0$, the value at the centre of mode shape is always zero. In Fig. 5, we display the normalized w_n corresponding to the first four natural frequencies ω_k^* $(k = 1\sim4)$ for $n = 1$ and 2 for various edge constraints.

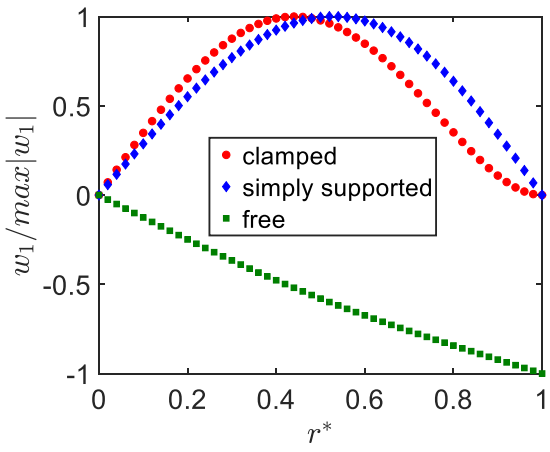
clamped
simply supported
free
$w_1/max|w_1|$
r^*

(a)

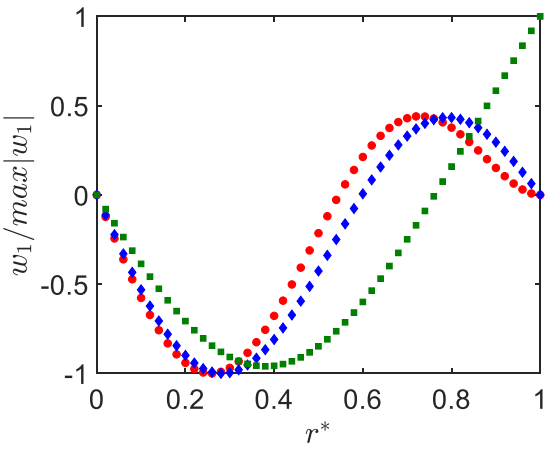
$w_1/max|w_1|$
r^*

(b)

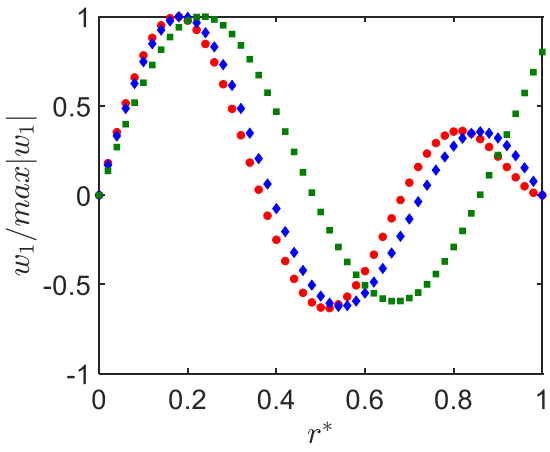
$w_1/max|w_1|$
r^*

(c)

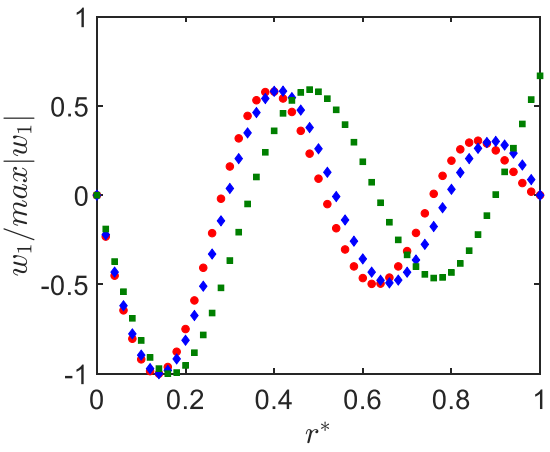
$w_1/max|w_1|$
r^*

(d)

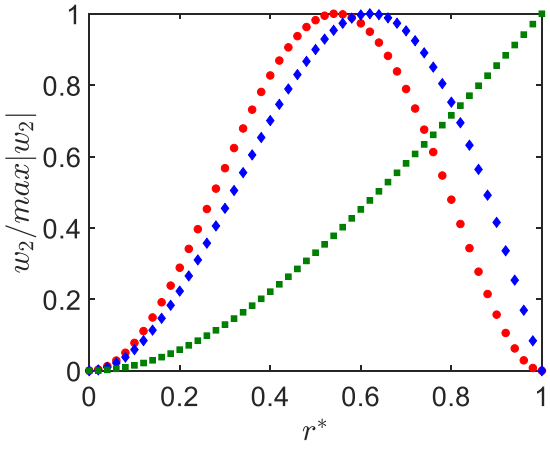
$w_2/max|w_2|$
r^*

(e)

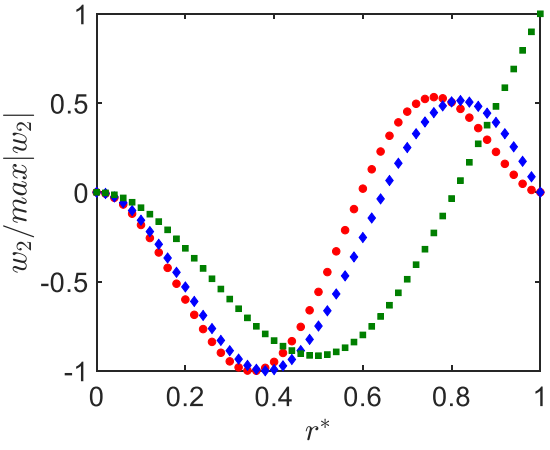
$w_2/max|w_2|$
r^*

(f)

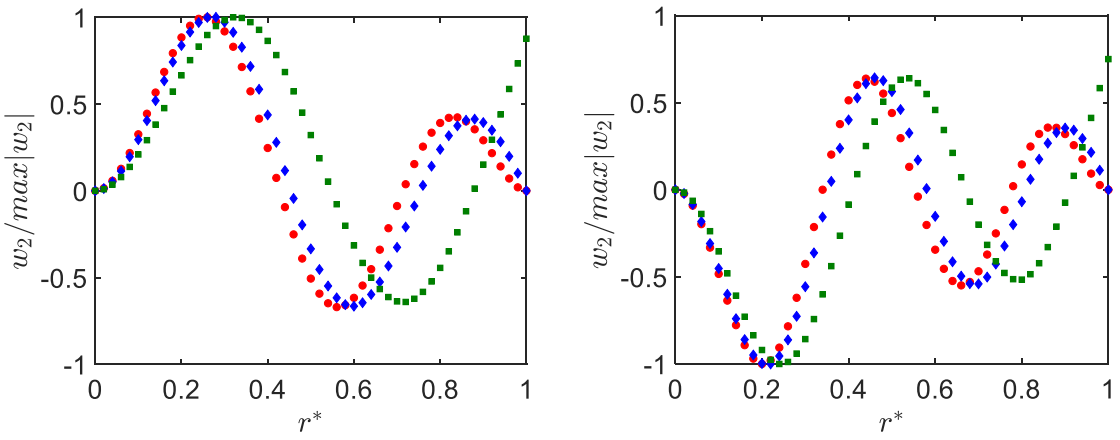

(g) (h)

Fig. 5. Normalized mode shapes corresponding to $n = 1$ and 2 for various edge conditions at the k^{th} natural frequency ω_k^* ($k = 1,2,3,4$) with $H^* = 1, L^* = 2 \times 10^{-3}, m^* = 1 \times 10^{-3}$. (a). $n = 1$ at ω_1^*; (b). $n = 1$ at ω_2^*. (c). $n = 1$ at ω_3^*; (d). $n = 1$ at ω_4^*; (e). $n = 2$ at ω_1^*; (f). $n = 2$ at ω_2^*. (g). $n = 2$ at ω_3^*; (h). $n = 2$ at ω_4^*.

For free edge case, it is observed that the maximum absolute values of the curves usually occur at the edge corresponding to the first two natural frequencies for both $n = 1$ and 2, while they are located at $0 < r^* < 0.5$ for cases corresponding to the third and fourth natural frequencies. For clamped and simply supported edge cases, the maximum absolute values of the curves occur at the first peak or trough.

We define

$$\widetilde{w}_n(r,\theta) = \cos n\theta \times \sum_{m=1}^{\infty} e_m J_n(\alpha_{nm} r), \tag{72}$$

based on which the mode shapes can be plotted. From Eq. (72), the zero deflection, or $\widetilde{w}_n(r,\theta) = 0$, is satisfied when either $w_n(r) = 0$ or $\cos n\theta = 0$, which correspond to nodal circles and nodal diameters (or nodal diametrical lines) in the context of free vibration of plates (e.g., Stuart and Carney [27]), respectively. It is obvious that in the area very close to a nodal point, there will be a very low level of vibration. The positions of nodal circles/diameters may well reflect the dynamic behaviours of the elastic plate and can be further used to study the vibration control. Here we may show the normalized mode shapes for clamped constraint in Fig. 6 at different modes (n, k), in which the nodal lines are shown as dashed-dotted curves. We can observe that the mode shapes

are anti-symmetric to the nodal diameters (at $n \geq 1$), and so it is also expected that the mode shape graphs become more oscillatory with the increase of n, as shown in Fig. 6.

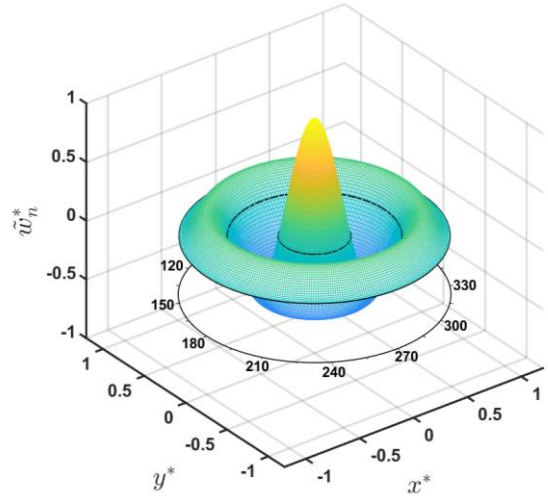

(a)

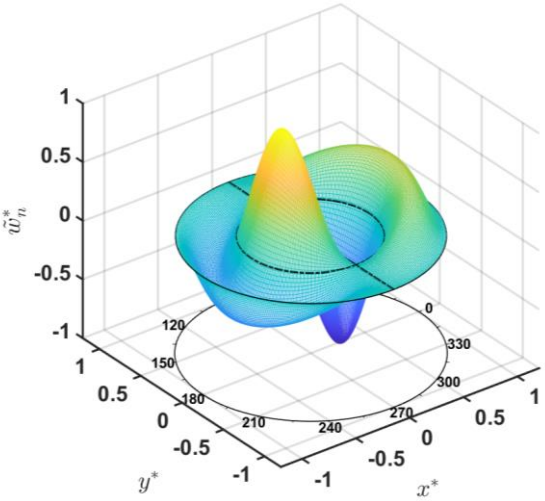

(b)

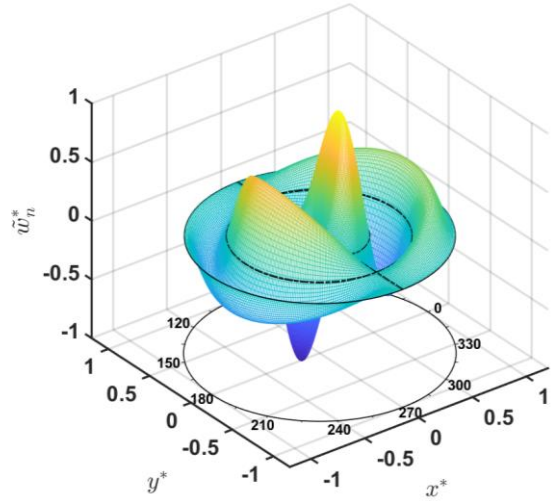

(c)

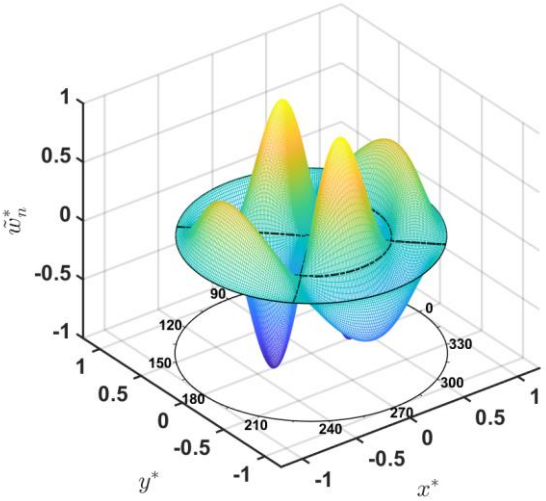

(d)

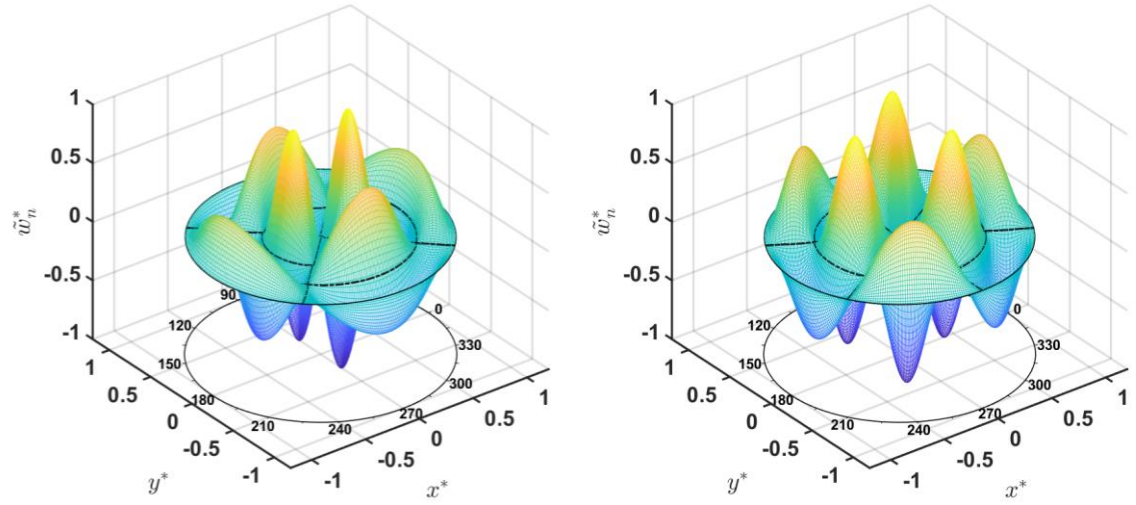

(e) (f)

Fig. 6. Normalized mode shapes for clamped edge with $H^* = 1$ at mode (n, k) with (n, k) equalling to: (a). (0,2); (b). (1,2); (c). (1,3); (d). (2,2); (e). (2,3); (f). (3,2).

4.4 Principal strains

The principal strain of the elastic cover can be obtained by calculating the eigenvalues of the strain tensor matrix (Fung [28])

$$\boldsymbol{\varepsilon} = \frac{h}{2}\begin{pmatrix} \varepsilon_{rr} & \varepsilon_{r\theta} \\ \varepsilon_{r\theta} & \varepsilon_{\theta\theta} \end{pmatrix} = \frac{h}{2}\begin{pmatrix} \dfrac{\partial^2 W}{\partial r^2} & \dfrac{1}{r}\dfrac{\partial^2 W}{\partial \theta \partial r} - \dfrac{1}{r^2}\dfrac{\partial W}{\partial \theta} \\ \dfrac{1}{r}\dfrac{\partial^2 W}{\partial \theta \partial r} - \dfrac{1}{r^2}\dfrac{\partial W}{\partial \theta} & \dfrac{1}{r}\dfrac{\partial W}{\partial r} + \dfrac{1}{r^2}\dfrac{\partial^2 W}{\partial \theta^2} \end{pmatrix}, \tag{73}$$

or the solution of $\det[\boldsymbol{\varepsilon} - \lambda \boldsymbol{I_2}] = 0$ with $\boldsymbol{I_2}$ being the identity matrix of size 2. We may choose one of the mode shapes for analysis. The expression of W may be written as

$$W(x, y, t) = \mathrm{Re}\{\widetilde{w}_n \times \mathrm{e}^{-i\omega t}\} = \widetilde{w}_n \cos \omega t, \tag{74}$$

by noticing that $\widetilde{w}_n$ is real. Therefore, we have

$$\lambda_{1,2} = \frac{h \cos \omega t}{4}\left\{C_1 \pm \sqrt{C_3^2 + 4C_2^2}\right\}, \tag{75}$$

where C_1, C_2 and C_3 are given as

$$C_1 = \cos n\theta \times \sum_{m=1}^{\infty} \frac{I_m}{\Omega_{nm}} J_n(\alpha_{nm} r),$$

$$C_2 = \sin n\theta \times \left\{n\mathcal{J}_0^{(n)} - n(n-1)\sum_{m=1}^{\infty} e_m \left[\frac{J_n(\alpha_{nm} r)}{r^2}\right]\right\},$$

$$C_3 = \cos n\theta \times \left\{ \sum_{m=1}^{\infty} \frac{I_m}{\Omega_{nm}} J_n(\alpha_{nm} r) + 2\mathcal{J}_0^{(n)} + 2n(n-1) \sum_{m=1}^{\infty} e_m \left[\frac{J_n(\alpha_{nm} r)}{r^2} \right] \right\}$$

with

$$\mathcal{J}_0^{(n)} = \sum_{m=1}^{\infty} e_m \left[\frac{\alpha_{nm} J_{n+1}(\alpha_{nm} r)}{r} \right].$$

Here J_n' has been replaced by J_{n+1} and J_n [23], and I_m is defined in Eq. (23). The term involving the summation of J_n in C_2 and C_3 is zero when $n = 0,1$ and non-singular at $r = 0$ when $n > 1$. It is also convergent. The series of $\mathcal{J}_0^{(n)}$ has no singularity at $r = 0$ but is not convergent and the way to treat its non-convergence is given in the Appendix A.

From Eq. (75), the maximum principal strain can be obtained as the maximum of $|\lambda_1|$ and $|\lambda_2|$ with $\cos \omega t = \pm 1$, or

$$\varepsilon_{max} = \frac{h}{4} \times \left\{ |C_1| + \sqrt{C_3^2 + 4C_2^2} \right\}. \tag{76}$$

The maximum principal strain along the radius is plotted in Fig. 7 for the axisymmetric case ($n = 0$) corresponding to the clamped, simply supported and free edge conditions, respectively. From Fig. 7, we can observe that for clamped edge, the maximum principal strain occurs at the tank wall for the first natural frequency. However, for other three natural frequencies, the maximum principal strains appear at the centre of the tank. Compared with the clamped edge case, the values at edges of other types are smaller than any other places and the largest values occur at $r^* = 0$. Besides, the values of ε_{max}^* are not monotonous with radius but a piecewise function based on Eq. (76), and the numbers of peaks increase with the increasing of the index k in ω_k^*. In addition, we may also find that the numbers of peaks for free edge case are less than the corresponding cases of clamped and simply supported edges.

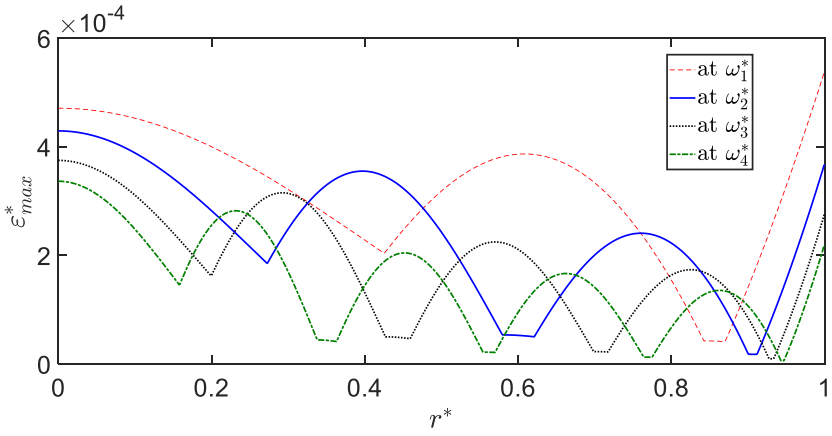

(a)

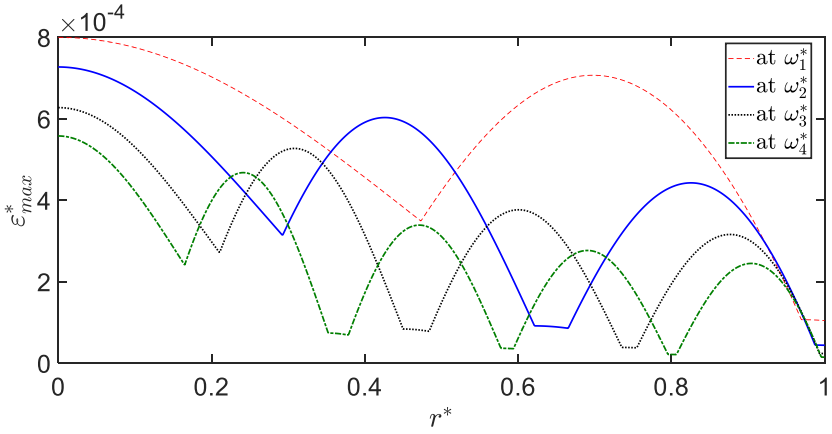

(b)

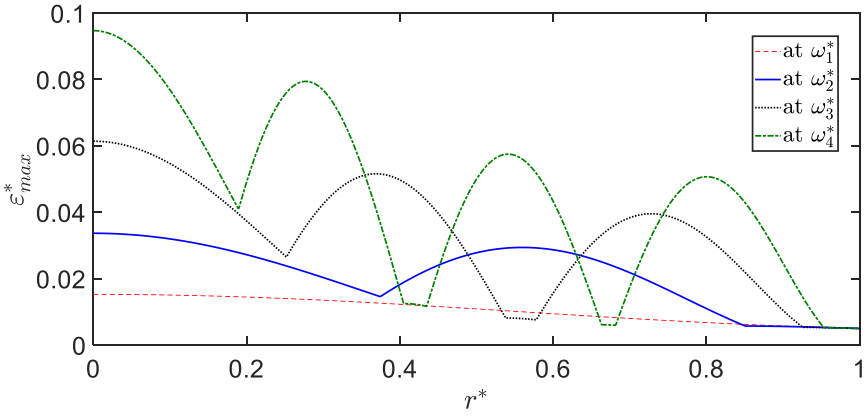

(c)

Fig. 7. Maximum principal strain of the clamped elastic cover corresponding to the given mode shapes at $n = 0$ with $H^* = 1, L^* = 2 \times 10^{-3}, m^* = 1 \times 10^{-3}, h^* = 10^{-2}$. (a). clamped edge at $\frac{\partial L^*_n}{\partial r^*}\Big|_{r^*=1} = 1$; (b). simply supported edge at $\frac{\partial L^*_n}{\partial r^*}\Big|_{r^*=1} = 1$; (c). free edge at $\frac{\partial w^*_n}{\partial r^*}\Big|_{r^*=1} = 1$.

For $n > 0$, the distribution of the maximum principal strains of the elastic cover with the clamped edge conditions is shown in Figs. 8 and 9 for $n = 1$ and $n = 2$, respectively. The graphs are symmetric about the centre and also the corresponding nodal diameter(s). These can be expected from Eq. (76). In fact we may write $\varepsilon_{max} = \frac{h}{4} \times \left\{ \mathscr{p}_n |\cos n\theta| + \sqrt{a_n^2 \cos^2 n\theta + \mathscr{b}_n^2 \sin^2 n\theta} \right\}$, where $\mathscr{p}_n$, a_n^2 and $\mathscr{b}_n^2$ are known from the expressions of C_1 to C_3 and $\mathscr{p}_n > 0$. From this, $\varepsilon_{max}(\theta, r) = \varepsilon_{max}(-\theta, r)$. Also for a nodal diametrical line at $\theta = \theta_0$, on which $\cos n\theta_0 = 0$ and $\sin n\theta_0 = \pm 1$, we have $\varepsilon_{max}(\theta_0 + \alpha, r) = \varepsilon_{max}(\theta_0 - \alpha, r)$. Besides, we can also observe that along the circumferential direction, ε_{max}^* has the minimal values at the nodal diametrical lines than at any other diametrical lines. At given radius r^*, we may further plot the maximum principal strain against different θ in Fig. 10 to show its variation. From the figure, we can find that the curves have sharp corners at $\theta = \pi/4, 3\pi/4, 5\pi/4$ and $7\pi/4$, which are the angles corresponding to the nodal diameters for $n = 2$.

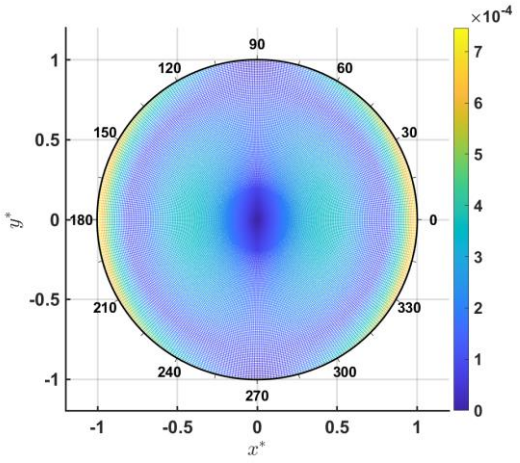

(a). ω_1^*

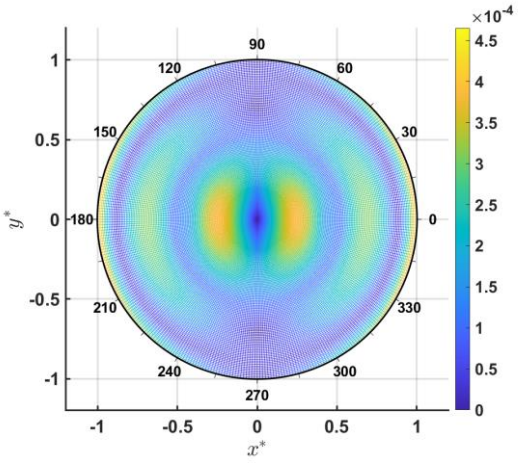

(b). ω_2^*

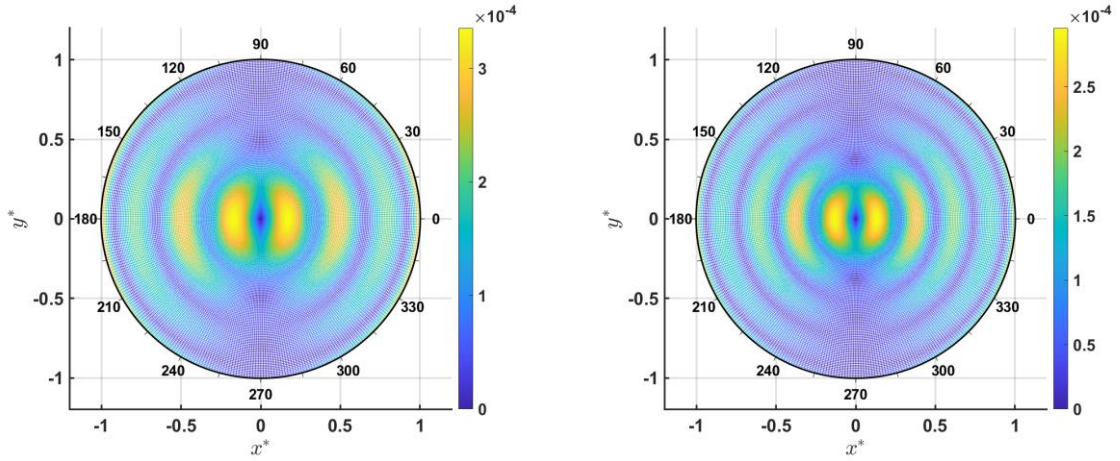

(c). ω_3^* (d). ω_4^*

Fig. 8. Maximum principal strain corresponding to mode shape at $n = 1$ with $H^* = 1, L^* = 2 \times 10^{-3}, m^* = 1 \times 10^{-3}, h^* = 1 \times 10^{-2}$, $\left.\frac{\partial L_n^*}{\partial r^*}\right|_{r^*=1} = 1$.

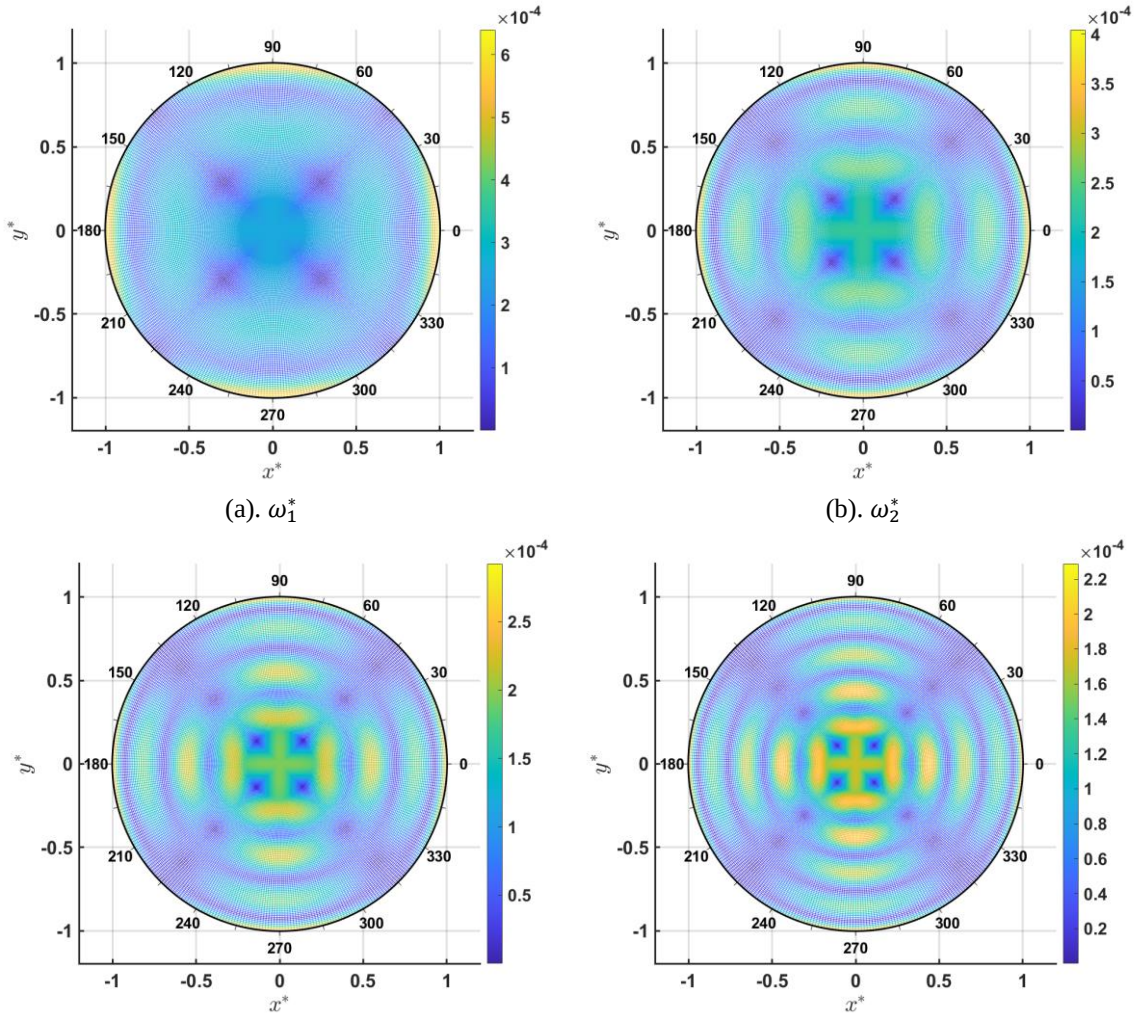

(a). ω_1^* (b). ω_2^*

(c). ω_3^* (d). ω_4^*

Fig. 9. Maximum principal strain of elastic cover corresponding to mode shape at $n = 2$ with $H^* = 1, L^* = 2 \times 10^{-3}, m^* = 1 \times 10^{-3}, h^* = 1 \times 10^{-2}$, $\left.\frac{\partial L_n^*}{\partial r^*}\right|_{r^*=1} = 1$.

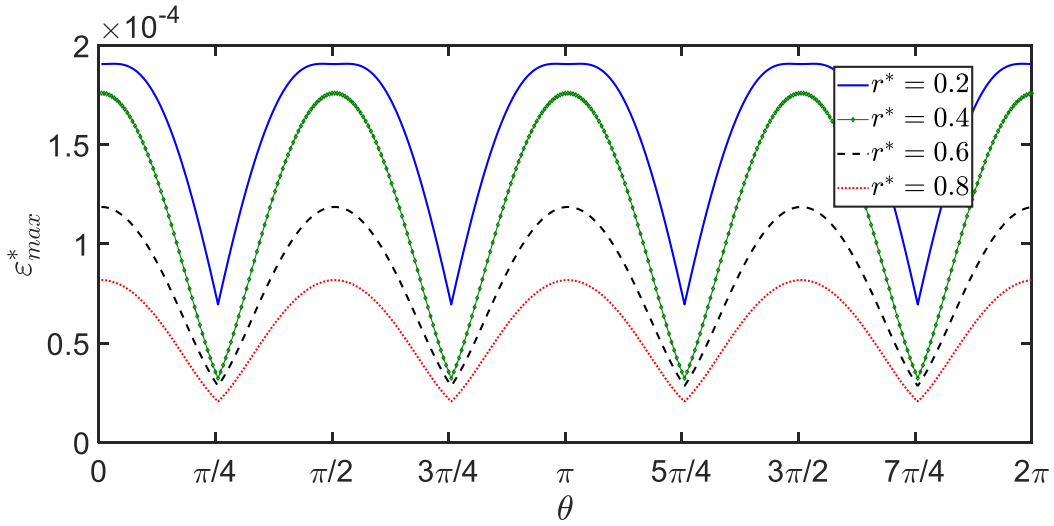

Fig. 10. Maximum principal strain against θ at different r^*, other parameters are same as those of Fig 9(d).

It is worth noting that the real motion of the system is the linear superposition of all the natural modes, which is further dependent on the initial conditions. In such a case, the deflection of the elastic cover can be obtained through the linear superposition of the natural mode shapes. However, the principal strain may not be obtained through directly superposition of the result for each natural mode, as the corresponding eigenvector of each mode may not be the same. For the calculation of the principal strain corresponding to certain initial conditions, the expression of W should be obtained first before using Eq. (73).

5. Conclusions

The natural modes of liquid motion coupled with an elastic plate on its upper surface in a cylindrical tank is investigated. Two effective solution schemes are developed, which are used to solve the problem for the plate with various edge constraints.

Explicit equations for the natural frequencies have been derived for the cover with different edge conditions and they are verified by a different method and residual theorem. The effect of various physical parameters on natural frequencies is

investigated. Increasing the liquid depth leads to an increase of the natural frequency but will approach the limit value very quickly. The natural frequency is very much affected by the nondimensionalized flexural rigidity L^* and mass per unit area m^*. Increasing L^* or decreasing m^* leads to an increase of natural frequencies for all the three edge types considered.

The natural frequency is independent to liquid density for free surface sloshing problem or sloshing without the elastic cover. The natural frequency of the coupling system with the cover is very much dependent on the liquid density. Specifically, as the liquid density becomes very large relative to that of the plate, the natural frequency of the system will tend to that of free surface without cover.

At higher natural frequencies, mode shapes along the axis direction is more oscillatory, due to larger bending moment and shear force, and subsequently a faster spatial variation of the deflection. The mode shapes also become more oscillatory when the numbers of nodal diameters n increases. For the distribution of maximum principal strains in the circular elastic cover, the values are symmetric about the centre and also the corresponding nodal diametrical line(s).

Acknowledgement

This work is supported by Lloyd's Register Foundation. The LRF helps protect life and property by supporting engineering-related education, public engagement, and the application of research. This work is also supported by the National Natural Science Foundation of China (Grant No. 52071162 and 51879123).

Appendix A. Dealing with non-convergent series

In C_2 and C_3 of Eq. (75), the infinite series $\mathcal{I}_0^{(n)}$ is non-convergent. We may write

$$\mathcal{I}_0^{(n)} = \sum_{m=1}^{\infty} e_m \frac{\alpha_{nm} J_{n+1}(\alpha_{nm} r)}{r} = \left.\frac{\partial L_n}{\partial r}\right|_{r=r_0} \times \frac{\mathcal{I}_1^{(n)}}{r} + \left.\frac{\partial w_n}{\partial r}\right|_{r=r_0} \times \frac{\mathcal{I}_2^{(n)}}{r}, \qquad \text{(A. 1)}$$

where

$$\mathcal{I}_1^{(n)} = \sum_{m=1}^{\infty} \frac{L r_0 \; J_n(\alpha_{nm} r_0)\; \alpha_{nm}\, J_{n+1}(\alpha_{nm} r)}{\left[\dfrac{\rho\omega^2}{\alpha_{nm}\tanh \alpha_{nm} H} \; - (L\alpha_{nm}^4 + \rho g - \rho_e h\omega^2)\right] \Omega_{nm}} \tag{A. 2}$$

and

$$\mathcal{I}_2^{(n)} = -\sum_{m=1}^{\infty} \frac{L r_0 \alpha_{nm}^3 \; J_n(\alpha_{nm} r_0)\, J_{n+1}(\alpha_{nm} r)}{\left[\dfrac{\rho\omega^2}{\alpha_{nm}\tanh \alpha_{nm} H} \; - (L\alpha_{nm}^4 + \rho g - \rho_e h\omega^2)\right] \Omega_{nm}} . \tag{A. 3}$$

We notice that in $\mathcal{I}_2^{(n)}$ when m is large, the m^{th} term is of order $1/\alpha_{nm}$ and as a result the summation may not converge. Thus, we may write

$$\mathcal{I}_2^{(n)} = \mathcal{J}^{(n)} + \sum_{m=1}^{\infty} \frac{r_0\, J_n(\alpha_{nm} r_0) J_{n+1}(\alpha_{nm} r) \left(\rho g - \rho_e h\omega^2 - \dfrac{\rho\omega^2}{\alpha_{nm}\tanh \alpha_{nm} H}\right)}{\left[\dfrac{\rho\omega^2}{\alpha_{nm}\tanh \alpha_{nm} H} \; - (L\alpha_{nm}^4 + \rho g - \rho_e h\omega^2)\right] \Omega_{nm}\, \alpha_{nm}} \tag{A. 4}$$

with

$$\mathcal{J}^{(n)} = \sum_{m=1}^{\infty} \frac{r_0\, J_n(\alpha_{nm} r_0) J_{n+1}(\alpha_{nm} r)}{\Omega_{nm} \alpha_{nm}}. \tag{A. 5}$$

After separating $\mathcal{J}^{(n)}$ from $\mathcal{I}_2^{(n)}$, the remaining summation in (A.4) is then convergent.

For (A.5), we may use Eq. (9.1.30) of Abramowitz and Stegun [23] and let $z = \alpha_{nm} x$, $\nu = n + 1$ and $k = 1$. Integrating with respect to x from 0 to x_0, this leads to

$$\frac{x_0^{n+1} J_{n+1}(\alpha_{nm} x_0)}{\alpha_{nm}} = \int_0^{x_0} x^{n+1} J_n(\alpha_{nm} x)\, dx. \tag{A. 6}$$

By expanding Dirac delta function into an infinite series of Bessel functions, we have

$$\delta(r - x) = \sum_{m=1}^{\infty} \frac{x J_n(\alpha_{nm} x)}{\Omega_{nm}} J_n(\alpha_{nm} r) = \begin{cases} 0, & r \neq x \\ \infty, & r = x \end{cases}, \tag{A. 7}$$

Multiplying (A.7) with x^n, integrating the result with respect to x from 0 to x_0, and further using (A.6), we have

$$\sum_{m=1}^{\infty} \frac{J_n(\alpha_{nm} r) J_{n+1}(\alpha_{nm} x_0)}{\Omega_{nm} \alpha_{nm}} = \frac{1}{x_0^{n+1}} \int_0^{x_0} \delta(r - x)\, x^n\, dx = \begin{cases} 0, & x_0 < r \\ \dfrac{r^n}{x_0^{n+1}}, & x_0 > r \end{cases} . \tag{A. 8}$$

Replacing r and x_0 with r_0 and r respectively in (A.8), and applying the result to (A.5), we obtain $\mathcal{J}^{(n)} = 0$, as $r < r_0$.

References

[1]. O.F. Rognebakke, O.M. Faltinsen, Coupling of sloshing and ship motions, J. Ship Res. 47 (2003) 208-221. doi:10.5957/jsr.2003.47.3.208

[2]. S. Mitra, C.Z. Wang, J.N. Reddy, B.C. Khoo, A 3D fully coupled analysis of nonlinear sloshing and ship motion, Ocean Eng. 39 (2012) 1-13. doi:10.1016/j.oceaneng.2011.09.015

[3]. K. Hatayama, Lessons from the 2003 Tokachi-oki, Japan, Earthquake for prediction of long-period strong ground motions and sloshing damage to oil storage tanks, J. Seismol. 12 (2008) 255-263. doi:10.1007/s10950-007-9066-y

[4]. A.E. Veldman, J. Gerrits, R. Luppes, J.A. Helder, J.P.B. Vreeburg, The numerical simulation of liquid sloshing on board spacecraft, J. Comput. Phys. 224 (2007) 82-99. doi:10.1016/j.jcp.2006.12.020

[5]. C. Farhat, E.K.Y. Chiu, D. Amsallem, J.S. Schotté, R. Ohayon, Modeling of fuel sloshing and its physical effects on flutter, AIAA J. 51 (2013) 2252-2265. doi:10.2514/1.J052299

[6]. M. Toumi, M. Bouazara, M.J. Richard, Impact of liquid sloshing on the behaviour of vehicles carrying liquid cargo, Eur J Mech A Solids. 28 (2009) 1026-1034. doi:10.1016/j.euromechsol.2009.04.004

[7]. O.M. Faltinsen, A numerical nonlinear method of sloshing in tanks with two-dimensional flow, J. Ship Res. 22 (1978) 193-202. doi:10.5957/jsr.1978.22.3.193

[8]. T. Nakayama, K. Washizu, The boundary element method applied to the analysis of two-dimensional nonlinear sloshing problems, Int. J. Numer. Meth. Engng. 17 (1981) 1631-1646. doi:10.1002/nme.1620171105

[9]. W. Chen, M.A. Haroun, F. Liu, Large amplitude liquid sloshing in seismically excited tanks, Earthquake Engng. Struct. Dyn. 25 (1996) 653-669. doi:10.1002/(SICI)1096-9845(199607)25:7<653::AID-EQE513>3.0.CO;2-H

[10]. F. Solaas, O.M. Faltinsen, Combined numerical and analytical solution for sloshing in two-dimensional tanks of general shape, J. Ship Res. 41 (1997) 118-129. doi:10.5957/jsr.1997.41.2.118

[11]. G.X. Wu, R. Eatock Taylor, Finite element analysis of two-dimensional non-linear transient water waves, Appl. Ocean Res. 16 (1994) 363-372. doi:10.1016/0141-1187(94)00029-8

[12]. G.X. Wu, Q.W. Ma, R. Eatock Taylor, Numerical simulation of sloshing waves in a 3D tank based on a finite element method, Appl. Ocean Res. 20 (1998) 337-355. doi:10.1016/S0141-1187(98)00030-3

[13]. O.M. Faltinsen, A.N. Timokha, An adaptive multimodal approach to nonlinear sloshing in a rectangular tank, J. Fluid Mech. 432 (2001) 167-200. doi: 10.1017/S0022112000003311

[14]. G.X. Wu, Second-order resonance of sloshing in a tank, Ocean Eng. 34 (2007) 2345-2349. doi: 10.1016/j.oceaneng.2007.05.004

[15]. R.A. Ibrahim, Liquid sloshing dynamics: theory and applications, Cambridge University Press, Cambridge, 2005.

[16]. O.M. Faltinsen, A.N. Timokha, Sloshing (Vol. 577), Cambridge University Press, Cambridge, 2009.

[17]. H.F. Bauer, Coupled frequencies of a liquid in a circular cylindrical container with elastic liquid surface cover, J. Sound Vib. 180 (1995) 689-704. doi: 10.1006/jsvi.1995.0109

[18]. M. Amabili, Vibrations of circular plates resting on a sloshing liquid: solution of the fully coupled problem, J. Sound Vib. 245 (2001) 261-283. doi: 10.1006/jsvi.2000.3560

[19]. Y.W. Kim, Y.S. Lee, Coupled vibration analysis of liquid-filled rigid cylindrical storage tank with an annular plate cover, J. Sound Vib. 279 (2005) 217-235. doi: 10.1016/j.jsv.2003.10.032

[20]. M.Y. Abdollahzadeh Jamalabadi, Analytical solution of sloshing in a cylindrical tank with an elastic cover, Mathematics 7 (2019) 1070. doi:10.3390/math7111070

[21]. S.P. Timoshenko, S. Woinowsky-Krieger, Theory of plates and shells, McGraw-Hill, New York, 1959.

[22]. K. Ren, G.X. Wu, Z.F. Li, Hydroelastic waves propagating in an ice-covered channel, J. Fluid Mech. 886 (2020) A18. doi:10.1017/jfm.2019.1042

[23]. M. Abramowitz, I.A. Stegun, Handbook of mathematical functions with formulas, graphs, and mathematical tables. Dover Publications, Inc, New York, 1965.

[24]. T. Sahoo, T.L. Yip, A.T. Chwang, Scattering of surface waves by a semi-infinite floating elastic plate, Phys. Fluids. 13 (2001) 3215-3222. doi: 10.1063/1.1408294

[25]. D.V. Evans, R. Porter, Wave scattering by narrow cracks in ice sheets floating on water of finite depth, J. Fluid Mech. 484 (2003) 143-165. doi:10.1017/S002211200300435X

[26]. T. Wah, Vibration of circular plates, J. Acoust. Soc. Am. 34 (1962) 275-281. doi: 10.1121/1.1928110

[27]. R.J. Stuart, J.F. Carney III, Vibration of edge reinforced annular plates, J. Sound Vib. 35 (1974) 23-33. doi: 10.1016/0022-460X(74)90035-2

[28]. Y.C. Fung, A first course in continuum mechanics, Prentice-Hall, Inc, New Jersey, 1977.